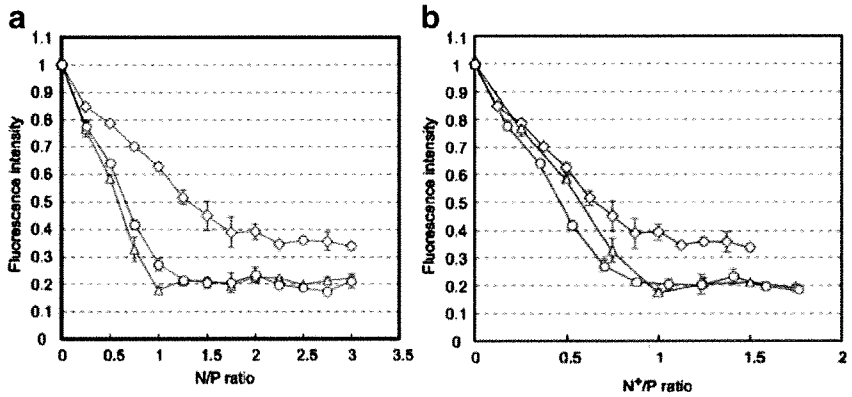

Fig. 3. EtBr dye exclusion assay on the polyplex micelles with varying compositions prepared from PAsp39(DET) (*diamonds*), PLys48 (*triangles*), and PAsp36(DET)Lys50 (*circles*; pDNA concentration, 10 μg/mL; EtBr concentration, 2.5 μg/mL; Temperature, 25°C; Medium, 10 mM Tris–HCl (pH 7.4) containing 150 mM NaCl). **a** The relationship with the N/P ratio, i.e., the residual molar ratio of amino groups in the polymer to phosphate groups in the pDNA. **b** The relationship with the N^+/P ratio, the residual molar ratio of protonated amino groups in the polymer to phosphate groups in pDNA at pH 7.4. Results were expressed as mean±SD (n=3).

To verify the influence of the order of the cationic components in the triblock copolymer, the zeta potential of the polyplex micelles from PEG–PLys–PAsp(DET) (the DPs of PLys and PAsp(DET) were 48 and 33, respectively) was also measured. As seen in Fig. 4d, the polyplex micelles from PLys48Asp33(DET) showed the similar level of zeta potential to those from PLys48. This indicates that PAsp (DET) aligned as an intermediate segment contributes to the higher zeta potential of the PAsp36(DET)Lys50 (Fig. 4b–d).

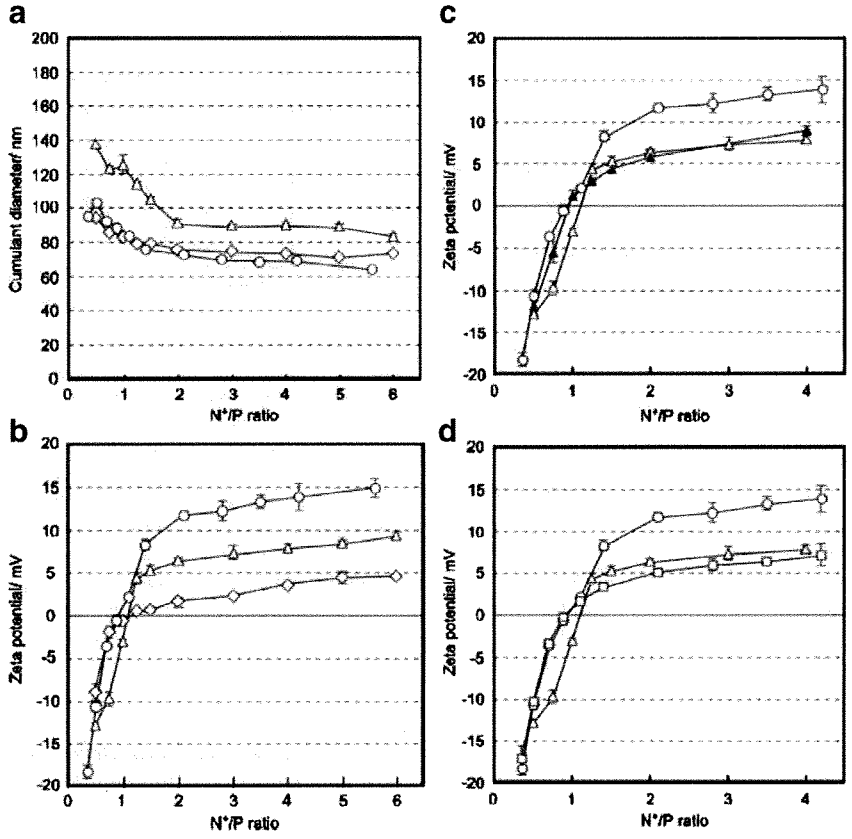

Fig. 4. Size and zeta potential of the polyplex micelles. **a** Size. **b**, **c**, **d** Zeta potential. PAsp39(DET); *diamonds*. PLys48; *empty triangles*. PLys109; *filled triangles*. PAsp36(DET) Lys50; *circles*. PLys48Asp33(DET); *squares*. (pDNA concentration, 33.3 μg/mL; Temperature, 37°C). Results were expressed as mean±SD (n=3).

In Vitro Transfection with Polyplex Micelles Prepared from Triblock Copolymer with Varying Polycations as an Intermediate Segment

Polyplex micelles were prepared from triblock copolymers with different polycation segments aligned between PEG and PLys segments and were subjected to a luciferase assay against Huh-7 cells in order to explore whether the change in the chemical composition of the intermediate polycation layer affects the transfection efficiency. As will be addressed in "DISCUSSION" section, the polyplex micelles from triblock copolymer is likely to take three layered structure at least in the region of excess polycation ($N^+/P>1$): the outer layer of PEG, the middle layer of buffering polycation, and the inner core of condensed PLys/pDNA polyplex (20). PLys segment, which is almost fully charged at physiological pH, is assumed to principally participate in the polyplex formation, keeping the intermediate polycation as free form in the middle layer of the micelles. Thus, it may be reasonable to compare the transfection efficiency of these polyplex micelles from the triblock copolymers with different intermediate segments at the fixed Lys/Phosphate ratio instead of N^+/P ratio, because the latter includes the contribution from the charged amino groups that may not directly participate in the polyplex formation. Here, the Lys/Phosphate ratio is fixed to 2 because the previous study revealed that pDNA condensation is completed at this ratio, exerting the optimal transfection efficiency (26).

The DPs of the intermediate polycations (PAsp(DAP), PAsp(APM), and PAsp(DET) as illustrated in Fig. 5a and the PLys in the triblock copolymers were fixed to 36 and 50, respectively, in this experiment. Fig. 5b clearly shows that the luciferase activity strongly depends on the structure of the intermediate polycation segments in the block copolymers. The polyplex micelles from the PAsp36(DAP)Lys50 showed a similar level of luciferase expression as those from the PLys48, indicating that the introduction of PAsp(DAP) segments with a similar pKa value, 9.9, to PLys had a negligible effect on the transfection efficacy. In line with our previous results (20), the polyplex micelles from the PAsp36(APM)Lys50 revealed some improvements in transfection efficacy compared to the PLys48 micelles. Notably, the highest transfection efficacy was achieved by polyplex micelles from the PAsp36(DET)Lys50, which showed tenfold higher luciferase activity than that from PLys48. On the other hand, the polyplex micelles from PEG–PLys–PAsp(DET) (the DPs of PLys and PAsp(DET) were 48 and 33, respectively), where the order of cationic segments between PAsp(DET) and PLys was inversed in the triblock copolymer, exhibited substantially decreased transfection efficacy compared with those from PAsp36(DET)Lys50.

The effect of the length of the cationic segments on the transfection efficacy was then studied in detail as seen in Fig. 5c. There was observed a critical increase in the transfection efficacy for PEG–PLys systems between the PLys20 and PLys48. It should be noted that one order of magnitude higher transfection was always obtained for the triblock systems compared to the diblock systems having similar total DPs of polycation segments (PLys71 *vs.* PAsp36(DET)Lys50 and PLys109 *vs.* PAsp66(DET)Lys47), supporting the result described in the preceding paragraph that the PAsp(DET) segment aligned as the intermediate segment plays a substantial role in the enhanced transfection.

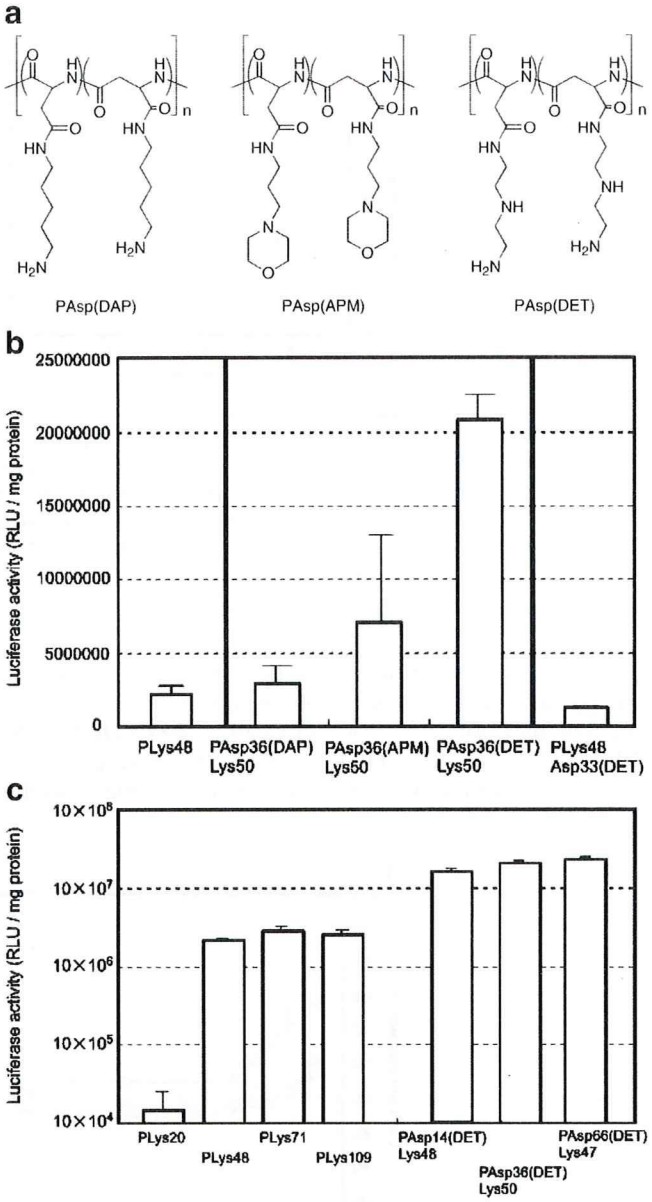

Fig. 5. Transfection efficacy of the polyplex micelles against Huh-7 cells (Luciferase assay). **a** Chemical structures of PAsp(DAP), PAsp (APM), and PAsp(DET) as the intermediate segment in the triblock copolymers. **b** Transfection efficacy of the polyplex micelles from PLys48, a series of triblock copolymers (PAsp36(R)Lys50) with varying intermediate segments (PEG–PAsp(DAP)–PLys, PEG–PAsp(APM)–PLys, and PEG–PAsp(DET)–PLys), and a triblock copolymer with the reversed order of the cationic segments, PLys48Asp33(DET). **c** Effect of the length of the cationic segments in di- or triblock copolymers on transfection efficacy. All the micelle samples were prepared at a Lys/Phosphate= 2 and applied for the transfection (pDNA concentration, 2.3 μg/mL).

Cellular Uptake and Intracellular Distribution of PEG–PAsp(DET)–PLys/pDNA Polyplex Micelles

From the results of luciferase assay, a PAsp(DET) segment integrated into the middle of the triblock copolymers was confirmed to improve the transfection activity of the polyplex micelles, consistent with the hypothesis of facilitated

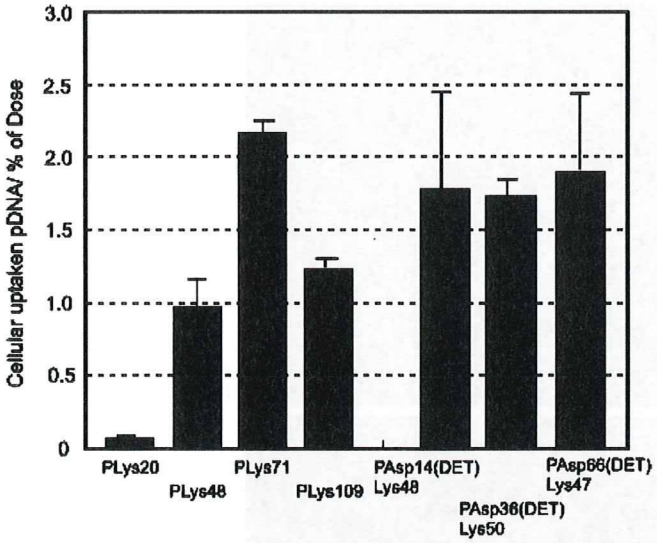

Fig. 6. Uptake into Huh-7 cells of ^{32}P-labeled pDNA in the polyplex micelles. All the micelle samples were prepared at a Lys/Phosphate = 2 and applied for the experiments (pDNA concentration, 2.3 μg/mL).

endosomal escape. Nevertheless, there is also a possibility that the higher zeta potential of PEG–PAsp(DET)–PLys micelles compared to other PEGylated systems (Fig. 4b,c) may facilitate their cellular uptake, leading to the improved transfection. Hence, a cellular uptake study was carried out using ^{32}P-labeled pDNA under a similar condition to the luciferase assay (Fig. 6). PLys20 micelle exhibited significantly lower uptake than those of other micelles, corresponding to its low transfection efficacy as shown in Fig. 5c. All of the micelles prepared from the diblock and triblock copolymers composed of PLys segments with DPs over 47 showed similar levels of cellular uptake. There was no significant difference in the efficacy of cellular uptake between the micelles with and without a PAsp(DET) segment as the middle block, excluding the facilitated cellular uptake as the reason for the improved transfection observed for the polyplex micelles from the triblock copolymers.

Then, intracellular distribution of the polyplex micelles from PLys48 and PAsp36(DET)Lys50 was observed by CLSM to estimate the efficacy of endosomal escape of the polyplex micelles. The pDNA, nuclei, and late endosomes/lysosomes were simultaneously stained with Cy5 (red), Hoechst33342 (blue), and LysoTracker (green), respectively. The Cy5-pDNA introduced into the PLys48 micelles without a PAsp(DET) segment was observed as discrete dots partially colocalizing with the late endosome/lysosome markers (yellow spots) 24 h after the addition of the polyplex micelles (Fig. 7a), indicating that the PLys48 polyplex micelles were segregated in intracellular compartments including late endosomes/lysosomes. In contrast, the Cy5-pDNA in PAsp36(DET)Lys50 polyplex micelles spread more clearly in the cytoplasmic region (Fig. 7b), demonstrating that effective endosomal escape had occurred. These results strongly support that the PAsp(DET) segment plays a crucial role in facilitating the endosomal escape of the polyplex micelles.

In Vivo Transfection by PEG–PAsp(DET)–PLys/pDNA Polyplex Micelle by Intravenous Administration

The transfection ability of the PAsp36(DET)Lys50 polyplex micelles by systemic administration was estimated from EGFP expression in subcutaneously xenografted human pancreatic adenocarcinoma, BxPC3. As previously reported, this tumor tissue has a poorly differentiated histology with a certain number of blood vessels and thick fibrotic tissue in the stroma (21); i.e., closely resembling the histology of certain intractable tumors observed in clinical specimens. The fluorescence microscopy of the sectioned xenografted tumors was obtained with immunostaining of tumor vasculature by PECAM-1 (red), and nuclear counter staining (blue; Fig. 8a). Apparently, the BxPC3 tumors were shown to have wide stromal regions (region S) surrounding nests of tumor cells (region T) and blood vasculature (region V). Fig. 8b shows the image of EGFP expression (green) in the BxPC3 tumor tissue receiving intravenous injection of the PAsp36(DET) Lys50 polyplex micelles incorporating pDNA coding for EGFP. The EGFP expression was evident, yet the intensity was very weak. Worth noting is that TβR-I inhibitor, which has been found to facilitate the accumulation of macromolecular drugs in tumor tissues (21), drastically improved the EGFP expression by the PAsp36(DET)Lys50 polyplex micelles (Fig. 8c). Note that the PAsp36(DET)Lys50 polyplex

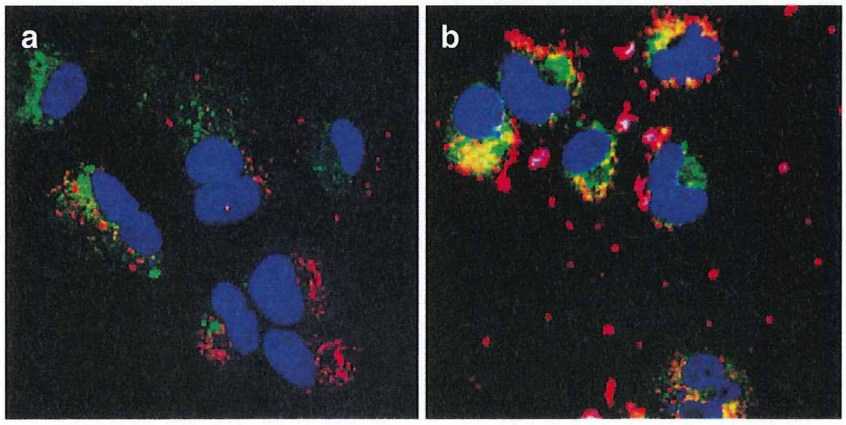

Fig. 7. Intracellular distribution of the PLys48 (**a**) and PAsp36(DET)Lys50 (**b**) micelles prepared at a Lys/Phosphate = 2. The pDNA was labeled with Cy5 (*red*), and the late endosomes/lysosomes and the nucleus were stained with LysoTracker (*green*) and Hoechst33342 (*blue*), respectively. (pDNA concentration, 2.8 μg/mL).

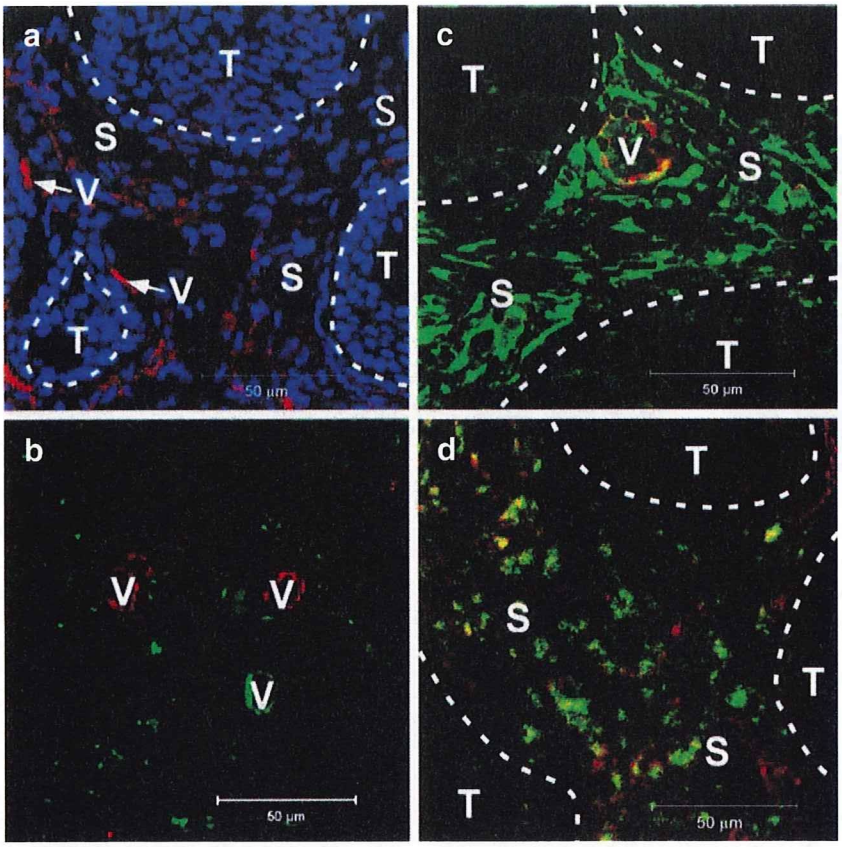

Fig. 8. EGFP transfection into subcutaneous tumors of pancreatic adenocarcinoma cells, BxPC3, *via* systemic route. Each micelle sample was prepared at a Lys/Phosphate=2, and intravenously injected through the tail veins of the mice (20 μg pDNA/mouse). **a** Histology of BxPC3 xenograft as a model of poorly differentiated pancreatic tumor tissue. *Blue*: nucleus stained with Hoechst 33342, *red*: PECAM-1 as an endothelial marker stained with Alexa647-conjugated secondary antibody against anti-PECAM-1 antibody (regions *T*, *S*, and *V* indicate nests of tumor cells in tumor tissues, thick fibrotic tissue in the stroma, and blood vasculature, respectively). **b** EGFP expression by PAsp36(DET)Lys50 polyplex micelle without TβR-I inhibitor; **c** EGFP expression by PAsp36(DET)Lys50 polyplex micelle with TβR-I inhibitor; **d** EGFP expression by PLys71 polyplex micelles with TβR-I inhibitor.

micelles in combination with TβR-I inhibitor did not show detectable EGFP expression in the liver and lung under the tested conditions (data not shown). Fig. 8d shows the result obtained for the PLys71 polyplex micelles with TβR-I inhibitor. Obviously, the EGFP expression by the PAsp36 (DET)Lys50 polyplex micelles was much more remarkable than that with the PLys71 polyplex micelles, suggesting that the integration of the PAsp(DET) segment into the polyplex micelles is effective even in the transfection by systemic administration. Detailed observation of the fluorescence images revealed that the EGFP expression by the polyplex micelles was located mainly around PECAM-1-positive vascular endothelial cells. As typically shown in Fig. 8a, the tumor stroma grows around the nests of tumor cells in BxPC3 subcutaneous xenografts, and blood vasculature exists inside the stroma. Therefore, a major part of the EGFP expression in the BxPC3 tumor by PAsp36(DET)Lys50 polyplex micelles was not from BxPC3 cells *per se*, but from cells in the stroma including vascular endothelial cells and fibroblasts.

DISCUSSION

In the present study, polyplex micelles with an endosomal escape layer were prepared from a triblock copolymer for the purpose of transfection into solid tumors through systemic routes. The triblock copolymer was composed of three tandemly aligned functional segments as follows: PEG for biocompatibility, PAsp(DET) for efficient endosomal escape, and PLys for pDNA condensation. A series of triblock copolymers, PEG–PAsp(DET)–PLys, with the DP of PLys of approximately 50, was synthesized and used for the preparation of the polyplex micelles, according to the previous results that a DP of approximately 48 was needed for effective transfection with polyplex micelles from PEG–PLys as shown in Fig. 5c as well as for the prolonged circulation of intact pDNA in the blood stream (10). The triblock copolymer, PAsp36(DET)Lys50, as well as the diblock PEG–PLys, PLys48, effectively condensed pDNA to form a polyplex micelle (Fig. 3). The obtained polyplex micelles

from the triblock copolymer were around 80 nm at an N^+/P ratio of 1 or greater (Fig. 4a), thereby having the potential ability to accumulate in tumors through the enhanced permeability and retention (EPR) effect (27). Also, the zeta potential measurement indicated that the excess positive charge of the polyplex micelle from the triblock copolymer was reasonably shielded by a PEG palisade surrounding the polyplex core (Fig. 4b). It should be noted that PEGylation of polyplexes facilitates their penetration into tumor spheroids (15, 16). Hence, the PEG palisade of polyplex micelles from the triblock copolymer may contribute to promoting their permeation into the tumor tissue *via* extravasation as well as to extending their plasma half-life through a steric stabilization effect, leading to appreciable gene expression in the subcutaneous pancreatic tumor tissue as seen in Fig. 8. Note that the xenografted pancreatic tumor, BxPC3, was chosen as our target in this study. Since pancreatic tumors are representative of intractable tumors, which are difficult to treat by conventional therapy, they are an appropriate target for the development of new strategies including gene therapy. However, it is also difficult to deliver exogenous genes to such tumor tissue by gene carriers through an EPR effect, presumably due to their thick fibrotic and hypovascular characteristics. In this regard, the combined use of TβR-I inhibitor, which has been found to decrease pericyte coverage of the endothelium specifically in tumor neovasculature (21), is available for the enhancement of accumulation of nanocarriers of 60–100 nm diameter into the solid tumor. Indeed, the EGFP expression by the polyplex micelles from PAsp36(DET)Lys50 was substantially improved by the intraperitoneal injection of TβR-I inhibitor (Fig. 8b,c). The size of the polyplex micelle was approximately 80 nm, thereby making it suitable for combination with TβR-I inhibitor. As far as we know, this is the first example of effective gene expression in BxPC3 tumors with thick fibrotic and hypovascular characteristics *via* systemic administration of non-viral vectors. In addition, detailed observation of the fluorescence images from sectioned xenografted tumors revealed that the EGFP expression by the PAsp36(DET)Lys50 polyplex micelle combined with TβR-I inhibitor was located mainly around the blood vasculature (Fig. 8c), suggesting that the transfection with the polyplex micelle was not effective for the tumor cells *per se*, but for the cells in the tumor stroma, including vascular endothelial cells and fibroblasts. These results suggest that the penetration of polyplex micelles into tumor microenvironments may still be a major challenge, even with the aid of TβR-I inhibitor for successful systemic transfection directly to the BxPC3 tumor cells. In this regard, for the gene therapy of pancreatic adenocarcinoma with thick fibrotic tissues, the approach of treating the tissues surrounding the nests of tumor cells would be more realistic than that directly targeting tumor cells *per se*, e.g., with a tumor suppressor gene to induce apoptosis. Antiangiogenic gene therapy is one of the typical "indirect" approaches to treating fibrotic tumors, and research in this direction on combination treatment using polyplex micelles and TβR-I inhibitor is now ongoing in our laboratory.

The contribution of the PAsp(DET) segment in the triblock copolymer to improved transfection without increased cytotoxicity was obvious from the results of both *in vitro* and *in vivo* transfection studies (Figs. 5, 8, and Table II). It should be noted that there is no significant difference in cellular uptake between the polyplex micelles from the triblock and diblock copolymers (Fig. 6), even though the former revealed almost one order of magnitude higher transfection efficacy than the latter. This result suggests that the major cause for the facilitated transfection with the polyplex micelles from the triblock copolymer may be in the intracellular stage. Indeed, the CLSM observation clearly revealed the facilitated endosomal escape of pDNA associated with the polyplex micelles from the triblock copolymer (Fig. 7), indicating the availability of PAsp(DET) as an endosomal escape element. PAsp(DET) is likely to form the middle layer between the PEG shell and the PLys/pDNA polyplex core in the micelles, because PLys with higher affinity to pDNA than PAsp(DET) is assumed to undergo preferential condensation of pDNA, relegating the PAsp(DET) segment to the boundary with the PEG layer. Increased freedom of PLys as an outer block with a free chain-end may also contribute to the preferential complexation with pDNA. Note that a similar three-layered structure was previously proposed by us for polyplex micelles prepared from PEG–PAsp(APM)–PLys based on the results of ^{1}H-NMR spectroscopy (20). The appreciably higher zeta potential of PAsp36(DET)Lys50 micelles in the region at an N^+/P ratio of 1 or greater is consistent with the formation of a cationic middle layer (Fig. 4b,c) that is not completely shielded by the outer PEG layer. Thus, the PAsp(DET) placed in the middle layer of polyplex micelles should exert endosomal escape ability for efficient transfection through strong buffering and/or a membrane-destabilizing effect based on the unique two-step protonation behavior of the 1,2-diaminoethane unit (13,15). On the other hand, as seen in Fig. 5b, the one order of magnitude lower transfection efficacy obtained by reversing the order of PLys and PAsp(DET) segments in the triblock copolymer is interesting. It is reasonable to consider that arrangement of the PLys segment, with its strong condensing power against pDNA, as the intermediate segment of the triblock copolymer may allow the PAsp(DET) segment to become embedded in the core of the polyplex micelles, resulting in the loss of buffering and/or membrane-destabilizing capacity. The zeta potential of the PEG–PLys–PAsp(DET) systems similar to that of the PEG–PLys systems also supports the disappearance of the intermediate buffering layer in the polyplex micelles from PEG–PLys–PAsp(DET) with the reversed order of the cationic segments (Fig. 4d).

CONCLUSION

For the achievement of systemic gene delivery to solid tumors with appreciable transfection efficacy, gene carriers are required to exert integrated functions including a stealth property in the blood stream to deliver intact pDNA into tumor tissues and permeate target cells with smooth translocation from endosomal compartments into the cytoplasm, subsequently releasing the pDNA to induce effective transcription. In the present study, to develop a gene carrier with such integrated functions, three segments with distinctive functions; i.e., PEG for biocompatibility, PAsp(DET) for endosomal escape, and PLys for pDNA condensation, were tandemly aligned in a polymer strand to form three-layered

polyplex micelles. The obtained micelles showed one order of magnitude higher transfection efficacy against Huh-7, compared to the micelles from the PEG–PLys diblock copolymer without any segments exerting an endosomal escape function. Notably, the polyplex micelle from the triblock copolymer achieved clear *in vivo* transfection of the EGFP gene in fibrotic pancreatic adenocarcinoma, BxPC3, through systemic administration. It should be emphasized that the EGFP expression in the pancreatic tumor was drastically enhanced by the intraperitoneal injection of TβR-I inhibitor prior to the micelle injection, and thus, the potential for combined therapy using polyplex micelles and TβR-I inhibitor for systemic transfection to solid tumors was clearly evidenced. Furthermore, detailed observation of the immunostained tumor tissues revealed that the EGFP expression by the triblock copolymer micelles was located mainly in the stromal tissues surrounding the nests of tumor cells. These results suggest that the triblock micelle is quite promising for fibrotic tumor treatments by the approach of transfecting the tissues surrounding tumor cells, including fibroblasts and endothelial cells, to express proteins inhibiting tumor angiogenesis.

ACKNOWLEDGEMENTS

This work was financially supported by the Core Research Program for Evolutional Science and Technology (CREST) from the Japan Science and Technology Corporation (JST) as well as by Special Coordination Funds for Promoting Science and Technology from the Ministry of Education, Culture, Sports, Science and Technology of Japan (MEXT).

REFERENCES

1. Wiley (2007) Gene Therapy Clinical Trials Worldwide, provided by the *J. Gene Med.* http://www.wiley.co.uk/genetherapy/clinical/ (accessed 17/01/08)
2. D. W. Pack, A. S. Hoffman, S. Pun, and P. S. Stayton. Design and development of polymers for gene delivery. *Nat. Rev. Drug Discov.* **4**:581–593 (2005) doi:10.1038/nrd1775.
3. E. Mastrobattista, M. A. E. M. van der Aa, W. E. Hennink, and D. J. A. Crommelin. Artificial viruses: a nanotechnological approach to gene delivery. *Nat. Rev. Drug Discov.* **5**:115–121 (2006) doi:10.1038/nrd1960.
4. E. Wagner. Strategies to improve DNA polyplexes for *in vivo* gene transfer: Will "artificial viruses" be the answer? *Pharm. Res.* **21**:8–14 (2004) doi:10.1023/B:PHAM.0000012146.04068.56.
5. Y. Kakizawa, and K. Kataoka. Block copolymer micelles for delivery of gene and related compounds. *Adv. Drug Deliv. Rev.* **54**:203–222 (2002) doi:10.1016/S0169-409X(02)00017-0.
6. S. Katayose, and K. Kataoka. Water-soluble polyion complex associates of DNA and poly(ethylene glycol)-poly(L-lysine) block copolymer. *Bioconjugate Chem.* **8**:702–707 (1997) doi:10.1021/bc9701306.
7. M. A. Wolfert, E. H. Schacht, V. Toncheva, K. Ulbrich, O. Nazarova, and L. W. Seymour. Characterization of vectors for gene therapy formed by self-assembly of DNA with synthetic block co-polymers. *Hum. Gene. Ther.* **10**:2123–2133 (1996) doi:10.1089/hum.1996.7.17-2123.
8. Y. H. Choi, F. Liu, J. Kim, Y. K. Choi, J. S. Park, and S. W. Kim. Polyethylene glycol-grafted poly-L-lysine as polymeric gene carrier. *J. Control. Release.* **54**:39–48 (1998) doi:10.1016/S0168-3659(97)00174-0.
9. K. Itaka, A. Harada, K. Nakamura, H. Kawaguchi, and K. Kataoka. Evaluation by fluorescence resonance energy transfer of the stability of nonviral gene delivery vectors under physiological conditions. *Biomacromolecules.* **3**:841–845 (2002) doi:10.1021/bm025527d.
10. M. Harada-Shiba, K. Yamauchi, A. Harada, I. Takamisawa, K. Shimokado, and K. Kataoka. Polyion complex micelles as a vector in gene therapy—pharmacokinetics and *in vivo* gene transfer. *Gene. Ther.* **9**:407–414 (2002) doi:10.1038/sj.gt.3301665.
11. O. Boussif, F. Lezoualc'h, M. A. Zanta, M. D. Mergny, D. Scherman, B. Demeneix, and J. Behr. A versatile vector for gene and oligonucleotide transfer into cells in culture and *in-vivo* polyethylenimine. *Proc. Natl. Acad. Sci. U. S. A.* **92**:7297–7301 (1995) doi:10.1073/pnas.92.16.7297.
12. M. Neu, D. Fischer, and T. Kissel. Recent advances in rational gene transfer vector design based on poly(ethylenimine) and its derivatives. *J. Gene Med.* **7**:992–1009 (2005) doi:10.1002/jgm.773.
13. N. Kanayama, S. Fukushima, N. Nishiyama, K. Itaka, W.-D. Jang, K. Miyata, Y. Yamasaki, U. Chung, and K. Kataoka. A PEG-based biocompatible block catiomer with high buffering capacity for the construction of polyplex micelles showing efficient gene transfer toward primary cells. *Chem. Med. Chem.* **1**:439–444 (2006) doi:10.1002/cmdc.200600008.
14. K. Masago, K. Itaka, N. Nishiyama, U. Chung, and K. Kataoka. Gene delivery with biocompatible cationic polymer: pharmacogenomic analysis on cell bioactivity. *Biomaterials.* **28**:5169–5175 (2007) doi:10.1016/j.biomaterials.2007.07.019.
15. M. Han, Y. Bae, N. Nishiyama, K. Miyata, M. Oba, and K. Kataoka. Transfection study using multicellular tumor spheroids for screening non-viral polymeric gene vectors with low cytotoxicity and high transfection efficiencies. *J. Control Release.* **121**:38–48 (2007a) doi:10.1016/j.jconrel.2007.05.012.
16. M. Han, Y. Bae, N. Nishiyama, and K. Kataoka. Gene delivery with poly(amino acid)-based block catiomer polyplex micelles against multicellular tumor spheroid. *Abstracts of 13th International Symposium on Recent Advances in Drug Delivery Systems*, Salt Lake City, UT, (2007b), pp. 128.
17. D. Akagi, M. Oba, H. Koyama, N. Nishiyama, S. Fukushima, T. Miyata, H. Nagawa, and K. Kataoka. Biocompatible micellar nanovectors achieve efficient gene transfer to vascular lesions without cytotoxicity and thrombus formation. *Gene. Ther.* **14**:1029–1038 (2007) doi:10.1038/sj.gt.3302945.
18. K. Itaka, S. Ohba, K. Miyata, H. Kawaguchi, K. Nakamura, T. Takato, U. Chung, and K. Kataoka. Bone regeneration by regulated *in vivo* gene transfer using biocompatible polyplex nanomicelles. *Mol. Ther.* **15**:1655–1662 (2007) doi:10.1038/sj.mt.6300218.
19. K. Miyata, S. Fukushima, N. Nishiyama, Y. Yamasaki, and K. Kataoka. PEG-based block catiomers possessing DNA anchoring and endosomal escaping functions to form polyplex micelles with improved stability and high transfection efficacy. *J. Control Release.* **122**:252–260 (2007) doi:10.1016/j.jconrel.2007.06.020.
20. S. Fukushima, K. Miyata, N. Nishiyama, N. Kanayama, Y. Yamasaki, and K. Kataoka. PEGylated polyplex micelles from triblock catiomers with spatially ordered layering of condensed pDNA and buffering units for enhanced intracellular gene delivery. *J. Am. Chem. Soc.* **127**:2810–2811 (2005) doi:10.1021/ja0440506.
21. M. R. Kano, Y. Bae, C. Iwata, Y. Morishita, M. Yashiro, M. Oka, T. Fujii, A. Komuro, K. Kiyono, M. Kamiishi, K. Hirakawa, Y. Ouchi, N. Nishiyama, K. Kataoka, and K. Miyazono. Improvement of cancer-targeting therapy, using nanocarriers for intractable solid tumors by inhibition of TGF-beta signaling. *Proc. Natl. Acad. Sci. U. S. A.* **104**:3460–3465 (2007) doi:10.1073/pnas.0611660104.
22. W. H. Daly, and D. Poche. The preparation of *N*-carboxyanhydrides of alpha-amino-acids using bis(trichloromethyl)carbonate. *Tetrahedron Lett.* **29**:5859–5862 (1988) doi:10.1016/S0040-4039(00)82209-1.
23. A. Koide, A. Kishimura, K. Osada, W. -D. Jang, Y. Yamasaki, and K. Kataoka. Semipermeable polymer vesicle (PICsome) self-assembled in aqueous medium from a pair of oppositely charged block copolymers: physiologically stable micro-/nanocontainers of water-soluble macromolecules. *J. Am. Chem. Soc.* **128**:5988–5989 (2006) doi:10.1021/ja057993r.
24. A. Harada, S. Cammas, and K. Kataoka. Stabilized α-helix structure of poly(L-lysine)-block-poly(ethylene glycol) in aque-

ous medium through supramolecular assembly. *Macromolecules.* **29**:6183–6188 (1996) doi:10.1021/ma960487p.

25. A. Harada, and K. Kataoka. Formation of polyion complex micelles in an aqueous milieu from a pair of oppositely-charged block copolymers with poly(ethylene glycol) segments. *Macromolecules.* **28**:5294–5299 (1995) doi:10.1021/ma00119a019.
26. K. Itaka, K. Yamauchi, A. Harada, K. Nakamura, H. Kawaguchi, and K. Kataoka. Polyion complex micelles from plasmid DNA and poly(ethylene glycol)-poly(L-lysine) block copolymer as serum-tolerable polyplex system: physicochemical properties of micelles relevant to gene transfection efficiency. *Biomaterials.* **24**:4495–4506 (2003) doi:10.1016/S0142-9612(03)00347-8.
27. Y. Matsumura, and H. Maeda. A new concept for macromolecular therapeutics in cancer chemotherapy: mechanism of tumoritropic accumulation of proteins and the antitumor agent SMANCS. *Cancer Res.* **46**:6387–6392 (1986).

Inhibition of endogenous TGF-β signaling enhances lymphangiogenesis

Masako Oka,[1] Caname Iwata,[1] Hiroshi I. Suzuki,[1] Kunihiko Kiyono,[1] Yasuyuki Morishita,[1] Tetsuro Watabe,[1] Akiyoshi Komuro,[1] Mitsunobu R. Kano,[1] and Kohei Miyazono[1]

[1]Department of Molecular Pathology, Graduate School of Medicine, University of Tokyo, Tokyo, Japan

Lymphangiogenesis is induced by various growth factors, including VEGF-C. Although TGF-β plays crucial roles in angiogenesis, the roles of TGF-β signaling in lymphangiogenesis are unknown. We show here that TGF-β transduced signals in human dermal lymphatic microvascular endothelial cells (HDLECs) and inhibited the proliferation, cord formation, and migration toward VEGF-C of HDLECs. Expression of lymphatic endothelial cell (LEC) markers, including LYVE-1 and Prox1 in HDLECs, as well as early lymph vessel development in mouse embryonic stem cells in the presence of VEGF-A and C, were repressed by TGF-β but were induced by TGF-β type I receptor (TβR-I) inhibitor. Moreover, inhibition of endogenous TGF-β signaling by TβR-I inhibitor accelerated lymphangiogenesis in a mouse model of chronic peritonitis. Lymphangiogenesis was also induced by TβR-I inhibitor in the presence of VEGF-C in pancreatic adenocarcinoma xenograft models inoculated in nude mice. These findings suggest that TGF-β transduces signals in LECs and plays an important role in the regulation of lymphangiogenesis in vivo. (Blood. 2008;111:4571-4579)

Introduction

Transforming growth factor-β (TGF-β) is a multifunctional cytokine, which regulates the growth, differentiation, migration, adhesion, and apoptosis of various types of cells. TGF-β binds to 2 different types of serine-threonine kinase receptors, known as type II (TβR-II) and type I (TβR-I).[1-3] Upon ligand binding, TβR-II transphosphorylates TβR-I, which in turn transmits specific intracellular signals. The type I receptors phosphorylate receptor-activated Smads (R-Smads), and induce complex formation between R-Smads and common-partner Smad (co-Smad). The R-Smad/co-Smad complexes accumulate in the nucleus, where they regulate transcription of target genes, including plasminogen activator inhibitor-1 (PAI-1) and Smad7, through interaction with various transcription factors and transcriptional coactivators. Smad2 and Smad3 are R-Smads activated by TβR-I, whereas Smad4 is the only co-Smad in mammals shared with the TGF-β family signaling pathways. Smad7 is an inhibitory Smad, which interacts with activated TβR-I and interferes with the phosphorylation of R-Smads by TβR-I.

TGF-β inhibits the growth and migration of blood vascular endothelial cells in vitro, whereas it induces angiogenesis in vivo.[4] Mice lacking certain components of TGF-β signaling (eg, TGF-β1, TβR-II, or TβR-I) exhibit abnormalities in blood vascular tissues.[5-7] We have recently shown that inhibition of TGF-β signaling by low-dose TβR-I inhibitor decreases the coverage of endothelium by pericytes, promoting leakiness of tumor blood vessels.[8] In tumor microenvironments, TGF-β signaling has also been reported to inhibit immune function and induce deposition of extracellular matrix proteins, inducing progression of tumors in advanced cancers.[9] However, the relationship between TGF-β signaling and lymphangiogenesis has not been determined.

Various growth factors have been reported to be involved in lymphangiogenesis. These include vascular endothelial growth factor (VEGF)-C and D, hepatocyte growth factor, and angiopoetin-1 and -2.[10-15] Neo-lymphangiogenesis has also been reported to be induced by receptor tyrosine kinases, for example, fibroblast growth factor receptor 3 (FGFR3) and platelet-derived growth factor receptor (PDGFR)-β.[13,16] Among members of the VEGF family, VEGF-A transmits signals through the tyrosine kinase receptors VEGF receptor-2 (VEGFR2) and VEGFR1, which mediate signals that are required for vasculogenesis and hematopoiesis.[17,18] VEGF-C and VEGF-D bind to VEGFR3 expressed on lymphatic vessels and mediate signals to LECs, although they also bind to VEGFR2.[19] Analysis of *Vegfc*-null mice has revealed that VEGF-C is essential for normal development of the lymphatic vessels.[20] Moreover, VEGF-C has been found to be expressed in various human cancers and to induce tumor metastasis through induction of angiogenesis and lymphangiogenesis.[21,22] VEGF-D also promotes metastatic spread of tumors through induction of lymphangiogenesis.[11]

Among transcription factors, Prox1, a homeobox transcription factor, has been well known as an important regulator of lymphangiogenesis. During embryonic development, LECs arise by sprouting from the cardinal veins and migrate toward VEGF-C to form the primary lymphatic plexus.[23] Prox1 is expressed in a subset of endothelial cells of the cardinal vein during embryonic development, and these cells sprout to form the primary lymphatic plexus.[24,25] In *Prox1*-null mice, migration of LECs from the veins is arrested, leading to a complete absence of the lymphatic vasculature. Prox1 induces the expression of various LEC markers, including VEGFR3, LYVE-1, podoplanin, and integrin α_9, and

Submitted October 25, 2007; accepted February 23, 2008. Prepublished online as *Blood* First Edition paper, February 29, 2008; DOI 10.1182/blood-2007-10-120337.

The online version of this article contains a data supplement.

The publication costs of this article were defrayed in part by page charge payment. Therefore, and solely to indicate this fact, this article is hereby marked "advertisement" in accordance with 18 USC section 1734.

represses that of blood vascular endothelial cell markers (eg, VEGFR2 and VE-cadherin) in endothelial cells.[26-28]

In the present study, we show that TGF-β regulates the growth, migration, and cord formation of human dermal lymphatic microvascular endothelial cells (HDLECs) in vitro. In addition to inhibiting the proliferation and migration of HDLECs, TGF-β signaling suppressed the expression of LEC-related genes, including Prox1 and LYVE-1, in these cells. Moreover, inhibition of endogenous TGF-β signaling induced early lymph vessel development in mouse embryonic stem (ES) cells, and enhanced lymphangiogenesis in a mouse chronic peritonitis model and pancreatic cancer xenograft models. The present findings suggest that endogenous TGF-β signaling negatively regulates lymphangiogenesis in inflammatory tissues as well as in certain tumor tissues.

Methods

Cell culture and reagents

HDLECs were obtained from Cambrex (Walkersville, MD), and cultured in EGM2-MV medium containing endothelial cell growth supplements with 5% fetal bovine serum (FBS; Cambrex). The murine ES cell line R1 (a kind gift of A. Nagy, Mount Sinai Hospital, Toronto, ON)[29] was cultured on mitomycin C-arrested mouse embryonic fibroblasts (Chemicon International, Temecula, CA) in stem cell medium (Knock-out DMEM, Invitrogen, Carlsbad, CA) supplemented with 15% FBS, 2 mM of L-glutamine (Invitrogen), 0.1 mM of 2-mercaptoethanol (Invitrogen), 0.1 mM of MEM nonessential amino-acids (Invitrogen), 50 U/mL of penicillin-streptomycin (Invitrogen), and 1000 U/mL of leukemia inhibitory factor (Chemicon International), and passaged every 48 hours. Inflammatory macrophages were collected from ascites fluid in BALB/c mice 4 days after induction of peritonitis by intraperitoneal injection of thioglycollate (enriched thioglycollate medium, 2 mL; BD Biosciences, Franklin Lakes, NJ). BxPC3 and MIA PaCa-2 human pancreatic adenocarcinoma cell lines were obtained from the American Type Culture Collection (Manassas, VA). BxPC3 cells were grown in RPMI 1640 supplemented with 10% FBS. MIA PaCa-2 cells were grown in DMEM with 10% FBS. Overexpression of VEGF-C in BxPC3 cells and that of TGF-β1 in MIA PaCa-2 cells were done using a lentiviral infection system (a kind gift from H. Miyoshi, RIKEN, Tsukuba, Japan). cDNA encoding VEGF-C,[30] active form of TGF-β1,[31] or green fluorescent protein (GFP) was inserted into the multicloning site of the lentiviral vector construct, pCSII-CMV-RfA, using pENTR according to standard protocol (Invitrogen). TβR-I inhibitors LY364947 and SB431542 were purchased from Calbiochem (La Jolla, CA) and Sigma-Aldrich (St Louis, MO), respectively. LY364947 was used as a TβR-I inhibitor, unless specifically described. TGF-β1 and TGF-β3 were purchased from R&D Systems (Minneapolis, MN). Cycloheximide was from Sigma-Aldrich. VEGF-A and VEGF-C were purchased from R&D Systems and Calbiochem, respectively.

Antibodies

Antibodies to LYVE-1, Prox1, and podoplanin were purchased from Abcam (Cambridge, United Kingdom), Chemicon International, and Research Diagnostic (Flanders, NJ), respectively. PECAM1 antibody and Mac-1 antibody were from BD PharMingen (Franklin Lakes, NJ). Rat anti–mouse LYVE-1 antibody was a kind gift from Y. Oike and T. Suda (Keio University, Tokyo, Japan). Antibody to phospho-Smad2 was a kind gift from A. Moustakas and C.-H. Heldin (Ludwig Institute for Cancer Research, Uppsala, Sweden). Antibodies to Smad2/3 and tubulin were from BD Transduction Laboratories (Franklin Lakes, NJ) and Sigma-Aldrich, respectively. Alexa488- and Alexa594-conjugated secondary antibodies and TOTO-3 were purchased from Invitrogen.

Immunoblotting

Cultured cells were lysed in a buffer containing 50 mM Tris-HCl, pH 8.0, 150 mM NaCl, 1% Nonidet P-40 (Nacalai Tesque, Kyoto, Japan), 5 mM EDTA, 0.5% deoxycholic acid sodium salt-monohydrate (Nacalai Tesque), 0.1% sodium dodecyl sulfate (SDS, Nacalai Tesque), 1% aprotinin (Mitsubishi Pharma, Osaka, Japan), and 1 mM phenylmethylsulfonyl fluoride (Sigma-Aldrich). The cell lysates were boiled in SDS sample buffer (100 mM Tris-HCl, pH 8.8, 0.01% bromophenol blue, 36% glycerol, 4% SDS, 10 mM dithiothreitol) and subjected to SDS-PAGE. Proteins were electrotransferred to PALL FLUOROTRANS W membranes (PALL, East Hills, NY), immunoblotted with antibodies, and detected using an ECL detection system (GE Healthcare, Little Chalfont, United Kingdom).

Immunostaining

Cultured cells were fixed in iced 1:1 acetone-methanol solution and incubated with antibody to Prox1 overnight at 4°C. Subsequently, cells were incubated with Alexa488-conjugated secondary antibodies (Invitrogen) for 1 hour at room temperature and stained with TOTO-3 for nuclear staining. Frozen sections were briefly fixed with Mildform 10N (WAKO, Osaka, Japan), and incubated with anti-LYVE-1, anti-Prox1, or anti-podoplanin antibodies. Subsequently, samples were incubated with secondary antibodies, and stained with TOTO-3 for nuclear staining. Stained cells and frozen sections were observed with a confocal microscope (Model LSM510 META; Carl Zeiss MicroImaging, Thornwood, NJ). Images were imported into Adobe Photoshop and analyzed using ImageJ software (National Institutes of Health, Bethesda, MD).

Enzyme-linked immunosorbent assay

Expression levels of TGF-β1 protein were determined using TGF-β1 human ELISA kit Quantikine 2nd Generation (R&D Systems), according to manufacturer's protocol. TGF-β3 at 1 ng/mL was used as the exogenous TGF-β ligand to avoid complication in detection of TGF-β1 by ELISA. Induction of TGF-β1 in HDLECs was similar between TGF-β1 and TGF-β3 at 1 ng/mL.

RNA isolation and quantitative RT-PCR

Total RNAs from HDLECs were extracted using the RNeasy Mini Kit (Qiagen, Valencia, CA). First-strand cDNAs were synthesized using the Quantitect Reverse Transcription kit (Qiagen) with random hexamer primers. Quantitative real-time reverse transcriptase–polymerase chain reaction (RT-PCR) analysis was performed using the 7500 Fast Real-Time PCR System (Applied Biosystems). The primer sequences used were as follows: human GAPDH: forward 5′-GAAGGTGAAGGTCGGAGTC-3′, reverse 5′-GAAGATGGTGATGGGATTTC-3′, human Prox1: forward 5′-CCCAGGACAGTTTATTGACCG-3′, reverse 5′-GGTTGTAAGGAGTTTGGCCCA-3′, human LYVE-1: forward 5′-AGCCTGGTGTTGCTTCTCACT-3′, reverse 5′-GGTTCGCCTTTTTGCTCACA-3′, human Smad7: forward 5′-CCTTAGCCGACTCTGCGAACTA-3′, reverse 5′-CCAGATAATTCGTTCCCCCTGT-3′, human PAI-1: forward 5′-GGCTGACTTCACGAGTCTTTC-3′, reverse 5′-GCGGGCTGAGACTATGACA-3′, human TGF-β1: forward 5′-AGTGGACATCAACGGGTTCAG-3′, reverse 5′-CATGAGAAGCAGGAAAGGCC-3′, human TGF-β2: forward 5′-CTGTCCCTGCTGCACTTTTGTA-3′, reverse 5′-TGTGGAGGTGCCATCAATACCT-3′, human TGF-β3: forward 5′-TGGAAGTGGGTCCATGAAACCTA-3′, reverse 5′-GATGCTTCAGGGTTAAGAGTGTTG-3′, and human/mouse VEGF-C: forward 5′-TTCCTGCCGATGCATGTCTAA-3′, reverse 5′-TGTTCGCTGCCTGACACTGT-3′.

Cell growth and cord formation assays

HDLECs (2×10^3 cells) were seeded in 96-well plates, and cell growth was quantified for 2 days by WST-1 assay (Nacalai Tesque) according to manufacturer's protocol. Formation of cord-like structures was determined in 3-dimensional gel assays, where 10^4 cells were mixed with type I-A collagen gel (Nitta Gelatin, Osaka, Japan) and seeded onto culture slide.

The formation of cord-like structures was examined using video microscopy for 3 days. At the end of observation, the lengths of the cord-like structures were quantified in the 3-dimensional assay as follows: 4 microscopic fields with 5 Z-axis planes in each condition were photographed, and the total lengths of cord-like structures were quantified as the mean of the sum of the lengths in the 5 planes in each of the 4 microscopic fields. Long-running video microscopic analysis of living cells on the 8-well culture slides (BD Falcon) was performed using a Leica (Deerfield, IL) DM IRB microscope equipped with a hardware-controlled motor stage. The video images were analyzed using ImageJ software. For quantification of images, 8 to 10 fields were evaluated for each mouse.

Cell migration assay

Migration of HDLECs was determined using a Boyden chamber (8 μm pore size, BD Biosciences) with type I collagen coat. HDLECs (5×10^4) were seeded in serum-free medium containing 0.2% BSA in the upper chamber. VEGF-C (50 ng/mL) was added as the chemoattractant to the lower chamber, while TGF-β1 at 1 ng/mL or TβR-I inhibitor at 3 μM was added to the upper chamber. After a 6-hour incubation, cells in the upper chamber were carefully removed using cotton buds and cells at the bottom of the membrane were fixed and stained with 0.5% crystal violet in 20% methanol. Quantification was performed by counting the stained cells in triplicate.

Three-dimensional collagen assays of mouse ES cells

Three-dimensional collagen assays using mouse ES cells were performed as described previously.[32,33] Briefly, R1 ES cells were trypsinized, resuspended in stem cell medium without leukemia inhibitory factor supplemented with 30 ng/mL VEGF-A at day 0. The cells were then cultured in drops hanging. After 4 days, when ES cells aggregated to form embryoid bodies, drops were collected and embryoid bodies were seeded on a layer of solidified collagen type I solution (Nitta Gelatin), and a second layer of collagen solution was added on top. After 3 hours, medium with or without 30 ng/mL VEGF-A and 30 ng/mL VEGF-C was added. Medium containing VEGF-A and C was replaced every second day. TβR-I inhibitor at 3 μM or TGF-β1 at 1 ng/mL was added every second day for one week, started from one week after seeding. After culturing for 2 weeks, whole-mount samples were incubated with anti-LYVE-1, anti-PECAM1, anti-Prox1, and Alexa-conjugated secondary antibodies overnight. Samples were examined using a Zeiss LSM510 Meta confocal microscope for immunohistochemistry. Quantification of LYVE-1 stained areas was performed in 5 fields on 3 embryoid bodies.

Chronic peritonitis model

BALB/c mice of 4 to 5 weeks of age were obtained from Sankyo Laboratory (Tokyo, Japan). All animal experimental protocols were performed in accordance with the policies of the Animal Ethics Committee of the University of Tokyo. Chronic peritonitis was induced by 5% thioglycollate. Thioglycollate (2 mL) and TβR-I inhibitor (LY364947, 1 mg/kg) were administered intraperitoneally to BALB/c mice 3 times a week. After injections of these reagents into mice for 2 weeks, the mice were killed and the diaphragms were excised, fixed with Mildform 10N for 1 hour at room temperature and washed with sucrose buffer (dissolved in phosphate-buffered saline [PBS]). Whole-mount samples were subsequently incubated with anti-LYVE-1, anti-Mac-1, and Alexa594-conjugated secondary antibodies overnight. Samples were examined using a Zeiss LSM510 Meta confocal microscope for immunohistochemistry.

Cancer xenograft models

BALB/c nude mice 5 to 6 weeks of age were obtained from CLEA Japan (Tokyo, Japan) and Sankyo Laboratory. Parental, or VEGF-C- or TGF-β1-expressing tumor cells (5×10^6) in 100 μL PBS were implanted subcutaneously into male nude mice and allowed to grow for 2 to 3 weeks to reach proliferative phase, before initiation of TβR-I inhibitor administration. TβR-I inhibitor LY364947, dissolved in 5 mg/mL in DMSO and diluted with 100 μL PBS, or the vehicle control, was injected intraperitoneally at 1 mg/kg, 3 times a week for 3 weeks. Excised samples were directly frozen in dry-iced acetone for immunohistochemistry. Frozen samples were further sectioned at 10-μm thickness in a cryostat and subsequently incubated with primary and secondary antibodies as described above. Samples were observed using a confocal microscope.

Results

TGF-β transduces signals in HDLECs

To study the effects of TGF-β on lymphangiogenesis, we first examined whether TGF-β transduces signals in HDLECs.[34] Specific small molecule inhibitors of TGF-β family type I receptor kinases ALK-4, -5, and -7 (TβR-I inhibitors, LY364947 and SB431542[35,36]) were used to suppress endogenous TGF-β family signaling. Immunoblot analysis using phospho-Smad2 antibody revealed weak phosphorylation of Smad2 in untreated HDLECs, and that 1 ng/mL of TGF-β1 enhanced the phosphorylation of Smad2 in these cells (Figure 1A). In contrast, 3 μM of LY364947 and SB431542 decreased the basal and TGF-β1-induced Smad2 phosphorylation.

The transcription induced by TGF-β in HDLECs was further examined by quantitative real-time (RT)-PCR analysis. TGF-β1 induced transcription of *SMAD7* and *PAI1*, and the TβR-I inhibitors strongly suppressed their transcription (Figure 1B,C), suggesting that TGF-β transduces signals in HDLECs and TβR-I inhibitors suppress the signals induced by endogenous TGF-β. We also examined the effects of TGF-β1 (1 ng/mL) and LY364947 and SB431542 (3 μM) on proliferation of HDLECs. TGF-β1 suppressed the growth of HDLECs, whereas TβR-I inhibitors enhanced their proliferation in the presence and absence of TGF-β1 (Figure 1D and data not shown). These findings indicate that HDLECs respond to TGF-β signals similarly to human umbilical vein endothelial cells (HUVECs; Figure S1, available on the *Blood* website; see the Supplemental Materials link at the top of the online article).

Next, production of TGF-β by HDLECs was examined at mRNA and protein levels. TGF-β induced the expression of TGF-β1 mRNA, whereas the TβR-I inhibitors suppressed it in the presence and absence of TGF-β1 (Figure 1E). Expression of TGF-β2 or TGF-β3 mRNA was not significantly suppressed by the TβR-I inhibitors (Figure S2). Moreover, ELISA revealed that HDLECs produce TGF-β1 protein at a level similar to that produced by HUVECs, and the secretion of TGF-β1 was stimulated and suppressed by exogenous TGF-β and TβR-I inhibitor, respectively (Figure 1F), suggesting the presence of autocrine loop of TGF-β1 signaling in HDLECs.

TGF-β induces expression of LEC markers in HDLECs

We next investigated whether TGF-β signaling regulates the expression of LEC markers in HDLECs. We recently reported that VEGFR3 signaling induces the expression of LYVE-1, but not other LEC markers, in embryonic stem cell (ESC)–derived endothelial cells.[30] In contrast, the homeobox transcription factor Prox1 induces expression of most LEC markers in ESC-derived endothelial cells.[28]

We examined the expression of Prox1 protein in HDLECs by immunocytochemistry and immunoblotting (Figure 2A,B). Prox1 was observed in the nuclei of most of the untreated HDLECs, although expression levels of Prox1 in them varied with some cells displaying very weak or no significant staining by Prox1 antibody (Figure 2A). When the cells were treated with TGF-β1 for

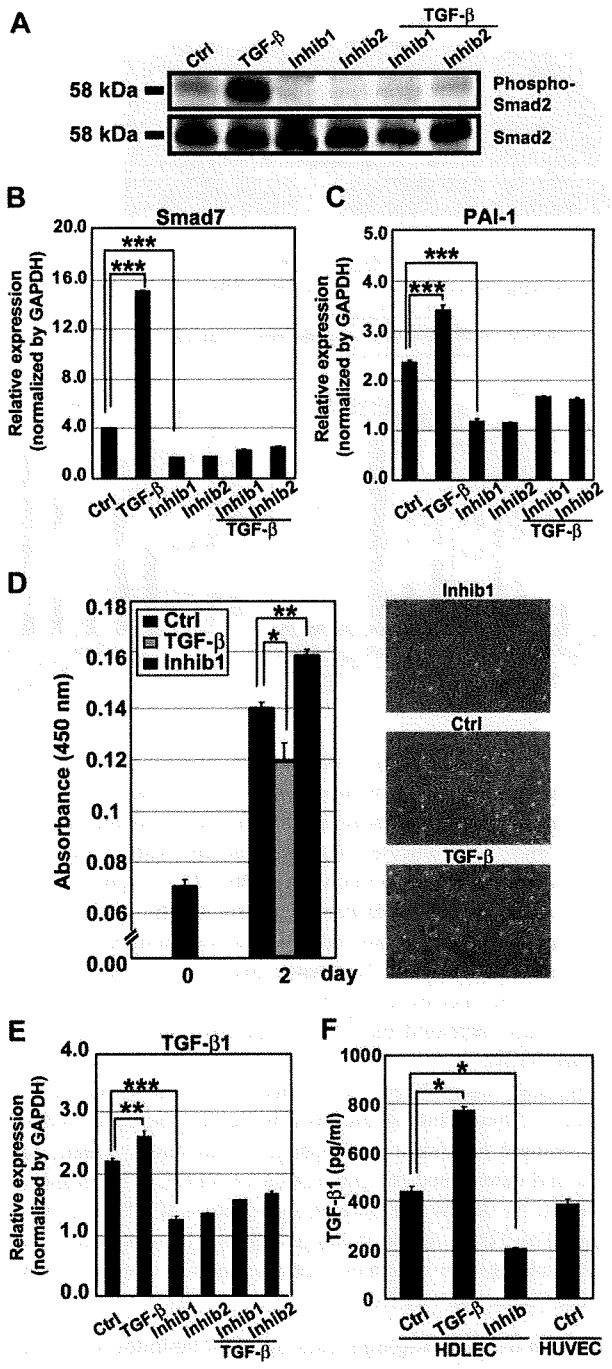

Figure 1. Transduction of TGF-β signals in HDLECs. (A) Immunoblotting of phospho-Smad2 after TGF-β or TβR-I inhibitor treatment. HDLECs were treated with TGF-β1 or with 2 kinds of TβR-I inhibitors (LY364947 or SB431542, shown as Inhib1 or Inhib2, respectively) in the presence and absence of TGF-β1 for 1 hour, and subjected to immunoblot analysis using phospho-Smad2 antibody (top panel) and Smad2/3 antibody (bottom panel). Ctrl indicates control. (B,C) Real-time PCR of Smad7 and PAI-1. HDLECs were treated as in panel A, and expression of Smad7 and PAI-1 mRNAs was determined at 1 hour and 24 hours after stimulation, respectively (***$P < .001$). (D) Regulation of growth of HDLECs by TGF-β and TβR-I inhibitor. HDLECs were seeded at a density of 2×10^3 cells/well in 96-well plates, and cells were treated or not with TGF-β1 (1 ng/mL) or LY364947 (3 μM). Photographs of the cells were taken at day 2. Cell numbers were determined by WST assay in triplicate at day 2. Error bars represent standard deviations (*$P < .05$, **$P < .01$). (E,F) Autocrine TGF-β signaling in HDLECs. Expression of TGF-β1 mRNA in HDLECs treated with TGF-β1 (1 ng/mL) or TβR-I inhibitors (3 μM) as in panel A was determined by real-time PCR (E). Production of TGF-β1 protein by HDLECs treated as in panel A, but with TGF-β3 (1 ng/mL) as the stimulant, was examined in conditioned medium using an ELISA kit (F). LY364947 was used as TβR-I inhibitor (Inhib). HUVECs were used as a control. Error bars represent standard deviations (*$P < .05$, **$P < .01$, ***$P < .001$).

24 hours, expression of Prox1 was strongly suppressed, and the number of cells with weak or no staining of Prox1 had increased. In contrast, TβR-I inhibitor LY364947 induced expression of Prox1 in almost all HDLECs after 24 hours. Immunoblot analysis using anti-Prox1 antibody confirmed the results of immunocytochemistry (Figure 2B).

Regulation of Prox1 expression as well as that of LYVE-1 by TGF-β signaling was further examined at the mRNA level. Total RNA was isolated from HDLECs treated with or without TGF-β1 or LY364947 for 24 hours, and levels of expression of Prox1 and LYVE-1 mRNAs were determined by quantitative RT-PCR (Figure 2C,D). TGF-β1 suppressed the expression of Prox1 and LYVE-1, whereas LY364947 strongly induced their expression. Similar results were obtained by another TβR-I inhibitor SB431542 (Figure S3A,B). The induction of Prox1 and LYVE-1 by TβR-I inhibitor was abolished by suppression of protein synthesis with cycloheximide treatment of HDLECs, whereas that of PAI-1 was not suppressed (Figure 2C-E). These findings suggest that TGF-β signaling indirectly regulates the expression of Prox1 and LYVE-1 in lymphatic endothelial cells. In contrast, Prox1 was not induced by TβR-I inhibitor in HUVECs, although LYVE-1 was up-regulated (Figure S3C,D).

Induction of cord formation and migration of HDLECs by TGF-β signaling

We examined the formation of cord-like structures by HDLECs in three-dimensional type I collagen gels. Quantification of the total length of cord-like structures after 3 days of cultivation confirmed significant decrease and increase in cord formation of HDLECs by treatment with TGF-β1 and TβR-I inhibitor, respectively (Figure 3A).

Next, migration of HDLECs was examined by Boyden chamber assay. HDLECs were treated or not with TGF-β1 or TβR-I inhibitor LY364947, and their migration toward VEGF-C (50 ng/mL) was determined after 6-hour incubation. In the absence of VEGF-C, migration of HDLECs was not strongly induced, and there was no significant difference in migration between untreated cells and those treated with TGF-β1 or TβR-I inhibitor (data not shown). VEGF-C induced the migration of HDLECs, which was strongly suppressed by TGF-β1, whereas TβR-I inhibitor weakly enhanced it (Figure 3B,C).

Induction of early lymph vessel development by TβR-I inhibitor in ES cells

To determine whether TGF-β signaling regulates lymphatic vessel development, mouse R1 ES cells were aggregated to form embryoid bodies, and cultured in three-dimensional collagen in the presence of VEGF-A and -C. Although VEGF-A and -C induced formation of lymphatic vessel structures as previously reported,[32,33] addition of TβR-I inhibitor LY364947 further induced the production of a network of LYVE-1-positive lymphatic vessel-like structures, whereas addition of TGF-β1 reduced the production of these structures (Figure 4A,B). Immunostaining of Prox1 in PECAM1-positive areas also increased with TβR-I inhibitor and decreased with TGF-β1 (Figure 4C), indicating that the effects of TGF-β signaling on lymphatics are not limited to HDLECs.

Inhibition of endogenous TGF-β signaling accelerates lymphangiogenesis in a mouse model of chronic peritonitis

We next examined whether inhibition of TGF-β signaling regulates lymphangiogenesis in vivo. Because chronic inflammation is

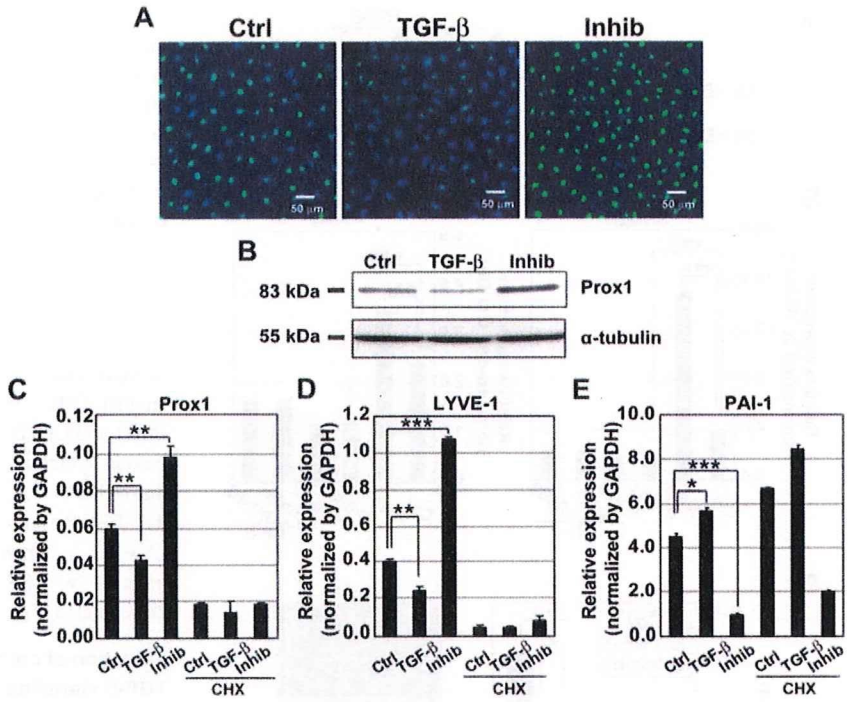

Figure 2. TGF-β signaling regulates the expression of LEC-related genes in HDLECs. (A) Expression levels of Prox1 determined by immunostaining in HDLECs. HDLECs were untreated (left) or treated with TGF-β1 (1 ng/mL; middle) or TβR-I inhibitor LY364947 (3 μM; right) for 24 hours and subjected to immunocytochemical examination. Bars represent 50 μm. (B) Expression levels of Prox1 in HDLECs treated as described in panel A were determined by immunoblotting. α-Tubulin levels were monitored as a loading control for whole-cell extracts. (C-E) Expression levels of Prox1, LYVE-1, and PAI-1 mRNAs were analyzed by real-time PCR at 24 hours after TGF-β1 or TβR-I inhibitor treatment. In the right 3 columns, cells were treated with 1 μM cycloheximide (CHX) for 24 hours before they were treated with TGF-β1 or TβR-I inhibitor for 24 hours. Values were normalized to amounts of GAPDH mRNA. Error bars represent SD (*$P < .05$, **$P < .01$, ***$P < .001$).

reported to induce lymphangiogenesis, possibly through production of VEGF-C by F4/80-positive macrophages,[37] we induced chronic peritonitis in mice as a model of lymphangiogenesis. Formation of inflammatory plaques containing lymphatic vessels and macrophages was induced on the peritoneal side of the diaphragm by intraperitoneal injection of thioglycollate in BALB/c mice. Mice were injected intraperitoneally with 2 mL of 5% thioglycollate and TβR-I inhibitor LY364947 (1 mg/kg) 3 times a week for 2 weeks. Lymphangiogenesis in the plaques of the diaphragms was then examined by immunostaining using LYVE-1 antibody. Formation of lymphatic plaques was observed after 2 weeks in the mice treated with thioglycollate, and TβR-I inhibitor significantly increased the LYVE-1-positive areas in the plaques (Figure 5A,B).

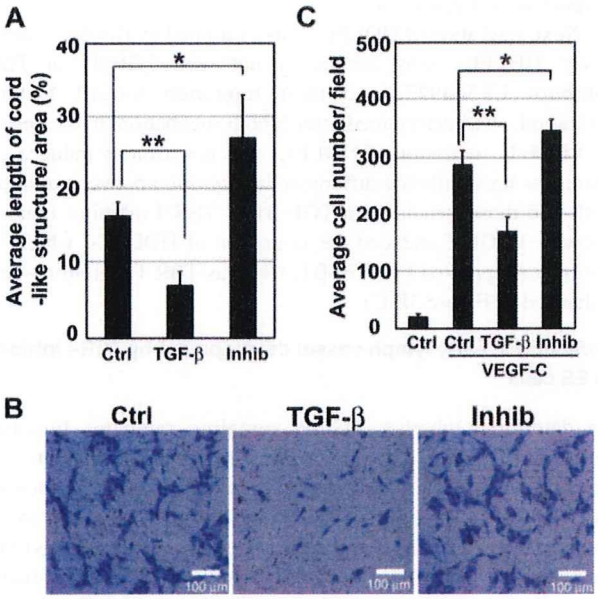

Figure 3. Formation of cord-like structures and migration of HDLECs are increased by inhibition of TGF-β signaling. (A) Total lengths of cord-like structures of HDLECs in three-dimensional culture were quantified. Cells were mixed with type I collagen gel at a density of 10^4 cells/well and seeded onto culture-slide wells. HDLECs were treated with TGF-β1 (1 ng/mL) or TβR-I inhibitor (3 μM). Formation of cord-like structures was observed by video microscopy, and total lengths of cord-like structures of cells were quantified 3 days after cultivation. Error bars represent SD (*$P < .05$, **$P < .01$). Effects of TGF-β signaling on migration of HDLECs were determined by Boyden chamber assay. Cells were seeded at 4×10^4 cells/well in the upper chambers coated with type I collagen. (B) Medium containing VEGF-C (50 ng/mL) was placed in the lower chamber, whereas that in the upper chamber did not contain VEGF-C but did contain TGF-β1 (1 ng/mL) or TβR-I inhibitor (3 μM). Migration of cells was determined after 6 hours. Bars represent 100 μm. (C) Migration of HDLECs was quantified. Cells that had migrated to the lower chambers were counted after 6 hours in triplicate. Error bars represent SD (*$P < .05$, **$P < .01$).

Because macrophages have been suggested to be the major sources of lymphangiogenic growth factors, including VEGF-C, we obtained peritoneal macrophages from thioglycollate-treated mice and determined the production of VEGF-C by quantitative RT-PCR. As shown in Figure 5C, production of VEGF-C was not induced by TβR-I inhibitor, suggesting that the observed effect of TβR-I inhibitor on lymphangiogenesis may be primarily induced by its direct action on LECs.

Induction of lymphangiogenesis by TβR-I inhibitor in animal models of cancer

Because TβR-I inhibitor induced growth, migration, and cord formation of LECs in vitro and lymphangiogenesis in a mouse model of chronic peritonitis in vivo, we examined whether it induces lymphangiogenesis in tumor xenograft models using BxPC3 and MIA PaCa-2 pancreatic adenocarcinoma cells. Pancreatic adenocarcinoma cells were inoculated subcutaneously into BALB/c nude mice. The mice were then injected with 1 mg/kg TβR-I inhibitor LY364947 3 times a week for 3 weeks.

When the BxPC3 cells were mixed with or without 1 μg/mL VEGF-C and inoculated into nude mice, we found that the number of LECs stained by LYVE-1 antibody was slightly increased in the presence of VEGF-C. Interestingly, TβR-I inhibitor significantly increased the LYVE-1-positive areas in tumor tissues in the presence of VEGF-C (Figure 6A,B). Z-stack

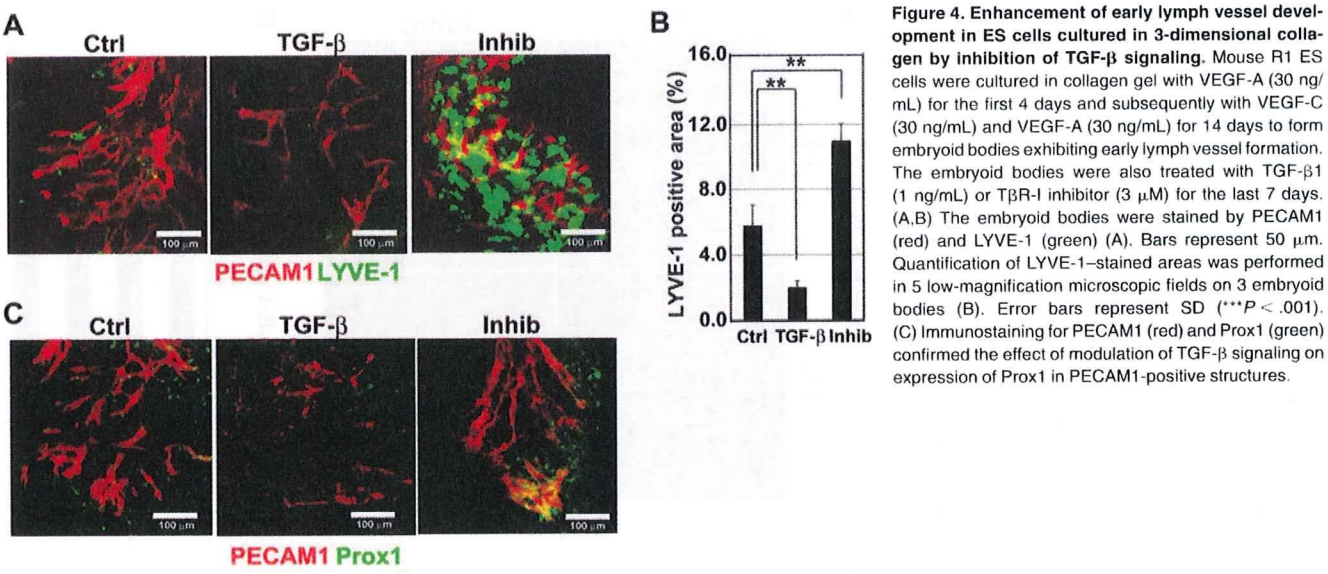

Figure 4. Enhancement of early lymph vessel development in ES cells cultured in 3-dimensional collagen by inhibition of TGF-β signaling. Mouse R1 ES cells were cultured in collagen gel with VEGF-A (30 ng/mL) for the first 4 days and subsequently with VEGF-C (30 ng/mL) and VEGF-A (30 ng/mL) for 14 days to form embryoid bodies exhibiting early lymph vessel formation. The embryoid bodies were also treated with TGF-β1 (1 ng/mL) or TβR-I inhibitor (3 μM) for the last 7 days. (A,B) The embryoid bodies were stained by PECAM1 (red) and LYVE-1 (green) (A). Bars represent 50 μm. Quantification of LYVE-1–stained areas was performed in 5 low-magnification microscopic fields on 3 embryoid bodies (B). Error bars represent SD (***$P < .001$). (C) Immunostaining for PECAM1 (red) and Prox1 (green) confirmed the effect of modulation of TGF-β signaling on expression of Prox1 in PECAM1-positive structures.

analysis of tumor tissues by a confocal microscope revealed that the LYVE-1-positive cells tended to form tube-like structures in the tumor tissues (data not shown). To confirm that the LYVE-1-positive cells were indeed LECs, tumor tissues treated with VEGF-C and TβR-I inhibitor were stained with Prox1 and podoplanin antibodies. The LYVE-1–postive cells were costained by Prox1 and podoplanin antibodies (Figure 6C), whereas most PECAM1-positive cells were not stained by LYVE-1 or Prox1 antibodies (Figure 6D). The LYVE-1–positive cells in the BxPC3 xenografts were thus LECs.

Similar experiments were conducted using BxPC3 cells overexpressing VEGF-C. BxPC3 cells were infected with a lentivirus containing *Vegfc*, and an increase in the production of VEGF-C mRNA by the VEGF-C-lentivirus-infected cells was confirmed by quantitative RT-PCR (Figure 6E). Similar to the addition of VEGF-C protein, TβR-I inhibitor significantly increased the LYVE-1–positive areas in BxPC3 tumor tissues expressing VEGF-C (Figure 6F).

The effects of TβR-I inhibitor on lymphangiogenesis were also examined using MIA PaCa-2 cells with or without 1 μg/mL VEGF-C protein. As shown in Figure 7, TβR-I inhibitor significantly increased the LYVE-1-positive areas in tumor tissues in the presence of VEGF-C. In addition, we have tested the effect of overexpression of TGF-β1 ligand in tumor cells using a lentivirus expression system in the MIA PaCa-2 model, which resulted in reduction of lymphangiogenesis (Figure S4).

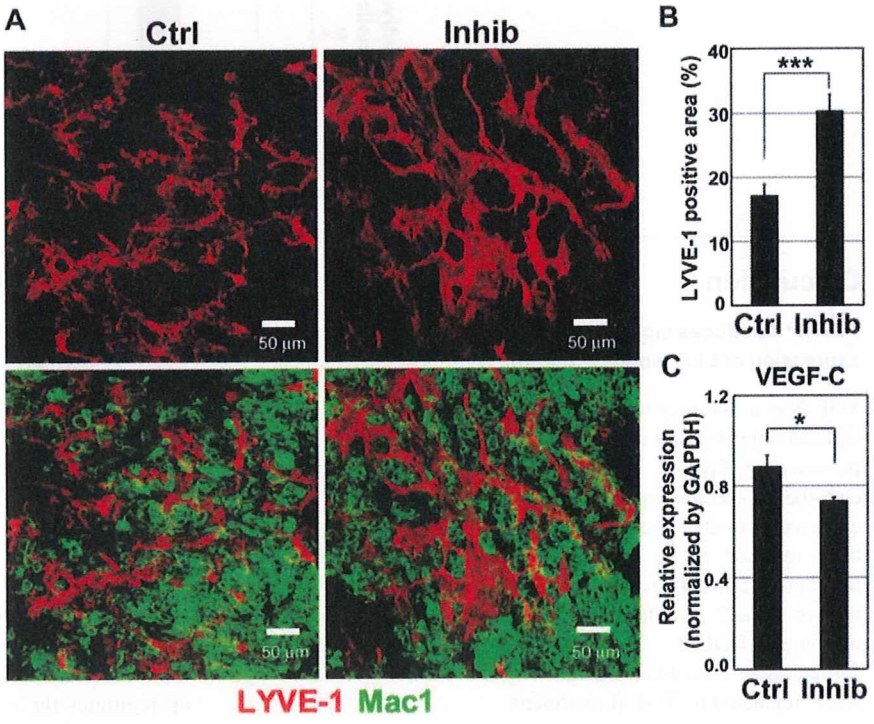

Figure 5. Enhancement of lymphangiogenesis by TβR-I inhibitor in a mouse model of chronic peritonitis. Mice were treated with 5% thioglycollate (2 mL) and TβR-I inhibitor (LY364947, 1 mg/kg) 3 times a week for 2 weeks. Their diaphragms were then examined for lymphangiogenesis in plaques. (A) LYVE-1 immunostaining (shown in red) of diaphragms treated without (control, left panels) or with TβR-I inhibitor (right panels). Sections were also stained for Mac1 (green) (bottom panels). Bars represent 50 μm. (B) Quantification of LYVE-1-positive area in plaques of the diaphragms treated without (control) or with TβR-I inhibitor ($n = 3$ for each group). Error bars represent SE (***$P < .001$). (C) Expression of VEGF-C in inflammatory macrophages in the presence and absence of TβR-I inhibitor. Inflammatory macrophages were harvested from ascites fluid of mice 4 days after induction of peritonitis by intraperitoneal injection of thioglycollate, seeded at 10^6, and treated with or without TβR-I inhibitor for 24 hours. Error bars represent SD (*$P < .05$).

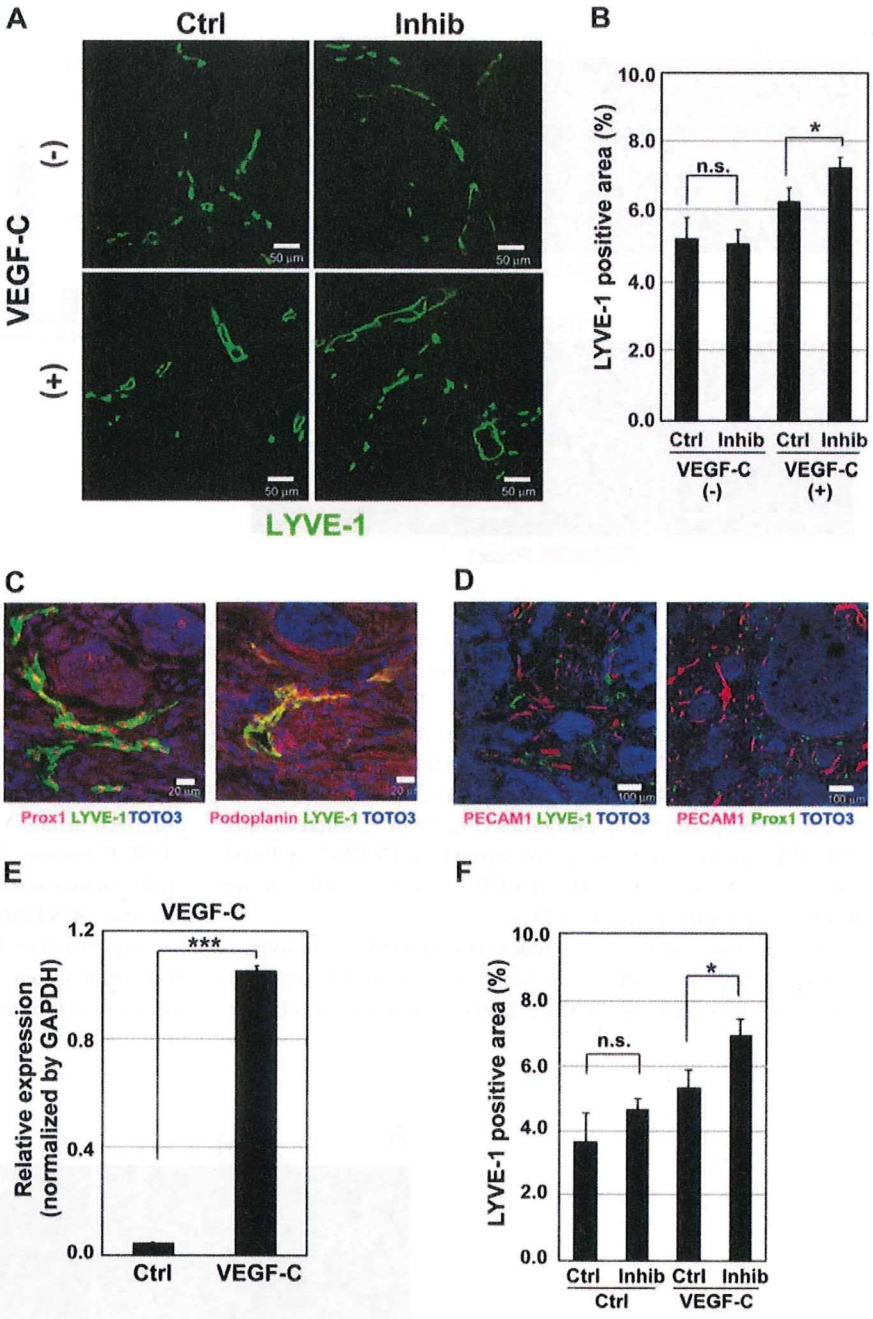

Figure 6. Lymphangiogenesis is increased by TβR-I inhibitor in pancreatic adenocarcinoma BxPC3 xenograft models. (A-D) Effects of TβR-I inhibitor on lymphangiogenesis were examined in a xenograft model using a human pancreatic cancer cell line, BxPC3. BxPC3 cells mixed with or without VEGF-C (1 μg/mL) were subcutaneously inoculated in BALB/c nude mice. After tumors had formed, the mice were injected intraperitoneally with TβR-I inhibitor (LY364947, 1 mg/kg) 3 times a week for 3 weeks. They were killed at the end of the experiment, and excised tumors were examined histologically. (A) Immunostaining of BxPC3 xenograft sections by LYVE-1 antibody (shown in green). Bars represent 50 μm. (B) LYVE-1–positive areas in the BxPC3 xenograft sections were determined in the presence and absence of VEGF-C and TβR-I inhibitor (n = 3 for each group). Error bars represent SE. n.s. indicates not significant (*$P < .05$). (C) Immunostaining of BxPC3 xenograft sections for Prox1 (left panel, red), podoplanin (right panel, red), and LYVE-1 (green). Bars represent 20 μm. (D) Immunostaining of BxPC3 xenograft sections for PECAM1 (red), LYVE-1 (left panel, green), Prox1 (right panel, green), and TOTO-3 (blue). Bars represent 100 μm. (E,F) Effects of TβR-I inhibitor on lymphangiogenesis were examined in a xenograft model using BxPC3 cells overexpressing VEGF-C by infection of the VEGF-C-lentivirus. BxPC3 cells infected with a lentivirus containing GFP were used as a control. (E) Up-regulation of VEGF-C mRNA in BxPC3 cells after infection of the VEGF-C-lentivirus was determined by real-time PCR. (F) LYVE-1-positive areas in the GFP- and VEGF-C–expressing BxPC3 xenograft sections treated with or without TβR-I inhibitor were determined (n = 3 for each group). Error bars represent SE. n.s. indicates not significant (***$P < .001$).

Discussion

TGF-β transduces signals in HDLECs and regulates the expression of LEC markers in vitro

TGF-β is a potent growth inhibitor on vascular endothelial cells and also inhibits their migration and cord formation in vitro. In the presence of TβR-II, TGF-β binds to TβR-I (ALK-5) and an endothelial-specific type I receptor ALK-1 in vascular endothelial cells, and activates Smad2/3 and Smad1/5, respectively. ALK-5 has been reported to be responsible for inhibition of growth and migration of endothelial cells.[38] We have found that phosphorylation of Smad2 is induced by TGF-β and suppressed by TβR-I inhibitor in HDLECs. Migration of HDLECs toward VEGF-C and formation of cord-like structures by these cells were thus negatively regulated by TGF-β treatment.

TGF-β also plays pivotal roles in regulating the differentiation of blood endothelial cells. Inhibition of endogenous TGF-β signaling by the TβR-I kinase inhibitor SB431542 results in the proliferation and formation of sheet-like structures of mouse ESC-derived endothelial cells.[39] In the present study, we found that TβR-I inhibitor up-regulated the expression of some LEC-related genes, including Prox1 and LYVE-1. We also found that TβR-I inhibitor induced early lymph vessel development in mouse ES cells. Thus, the effects of TβR-I inhibitor on LECs are not limited to HDLECs.

LYVE-1 is a hyaluronan receptor specifically expressed in LECs. However, LYVE-1–deficient mice do not exhibit abnormalities in lymphatic vessels, and the function of LYVE-1 in LECs is unknown.[40] In contrast, Prox1 functions as a key transcriptional factor in the differentiation of LECs. Prox1 up-regulates the expression of various LEC-specific genes and

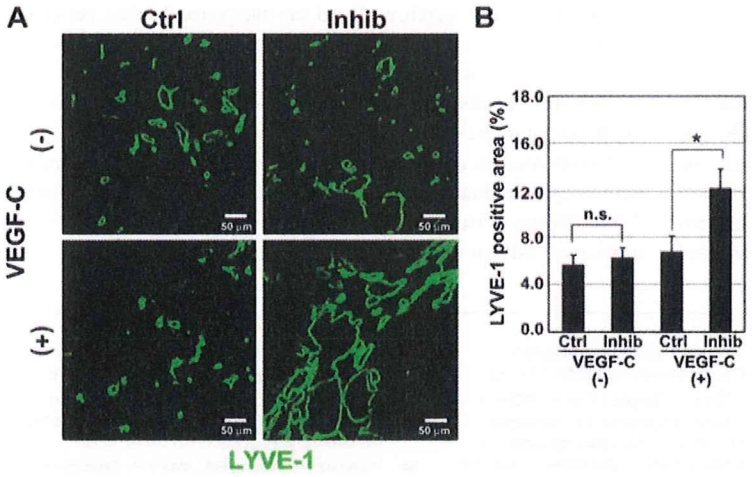

Figure 7. Induction of lymphangiogenesis by TβR-I inhibitor in MIA PaCa-2 xenograft models. (A,B) Effects of TβR-I inhibitor on lymphangiogenesis were examined in a xenograft model using a TGF-β–nonresponsive human pancreatic cancer cell line, MIA PaCa-2. MIA PaCa-2 cells mixed with or without VEGF-C (1 μg/mL) were subcutaneously inoculated in BALB/c nude mice and treated with TβR-I inhibitor (1 mg/kg) as described in Figure 7. Bars represent 50 μm. (A) Immunostaining of MIA PaCa-2 xenograft sections by LYVE-1 (shown in green). (B) LYVE-1–positive areas in the MIA PaCa-2 xenograft sections in the presence or absence of VEGF-C and TβR-I inhibitor were determined (n = 3 for each group). Error bars represent SE. n.s. indicates not significant (*$P < .05$).

induces a shift in the transcriptional program from blood endothelial cells to that of LECs. During embryonic development, Prox1 is expressed in a subset of vein endothelial cells, which begin to express LEC markers and form primary lymphatic sacs.[24,25] Elucidation of the signals that induce expression of Prox1 in blood endothelial cells is thus important to understand the mechanisms of lymphangiogenesis. VEGFR3 signaling does not induce the expression of Prox1,[30] whereas interleukin-3 signaling has been reported to induce expression of Prox1 in dermal blood endothelial cells.[41] Infection by Kaposi sarcoma-associated herpes virus also induces Prox1 expression in human dermal microvascular endothelial cells.[42] However, signaling pathways that regulate the expression of Prox1 in LECs have not been fully determined. The finding that TβR-I inhibitor induces the expression of Prox1 in HDLECs suggests that TGF-β signaling is a novel pathway that regulates Prox1 expression.

Induction of lymphangiogenesis by TβR-I inhibitor in vivo

We have shown that TβR-I inhibitor induces lymphangiogenesis in a chronic peritonitis model and in pancreatic carcinoma xenograft models. We used a low dose of TβR-I inhibitor for in vivo treatment, which has been shown to decrease the coverage of endothelium by pericytes and promote efficient accumulation of macromolecules to tumors through leakiness of tumor blood vessels. The low-dose TβR-I inhibitor acted on blood cells and vascular cells and suppressed the phosphorylation of Smad2 in these cells but not in tumor cells.[8] It will thus be of interest to examine whether the low-dose TβR-I inhibitor also acts on LECs and regulates lymphangiogenesis.

In the chronic peritonitis model we examined, lymphangiogenesis was induced in the diaphragm of immunocompetent mice through induction of chronic inflammation by repeated injection of thioglycollate. Accumulation of inflammatory cells (eg, macrophages) and LECs could be observed in the plaques.[43] Some LECs were positive for Ki-67, suggesting that these LECs were actively proliferating. Under these conditions, TβR-I inhibitor was able to induce lymphangiogenesis without addition of exogenous growth factors. Macrophages may produce VEGF-C[37] and other cytokines in sites of chronic inflammation; however, TβR-I inhibitor did not enhance the secretion of VEGF-C from inflammatory macrophages in the present study, suggesting that it may primarily induce lymphangiogenesis through direct action on LECs.

TβR-I inhibitor induced lymphangiogenesis in both xenografts of BxPC3 and those of MIA PaCa-2 cells in the presence of VEGF-C, suggesting that TβR-I inhibitor may induce proliferation of LECs once lymphatic vessels have been formed in the tumors by VEGF-C. An important question is whether TβR-I inhibitor induces lymphatic metastasis of tumors. The present findings suggest that TβR-I inhibitor may induce lymphangiogenesis in tumors that express VEGF-C or -D. However, Laakkonen et al reported that only certain types of cancers secrete VEGF-C.[21] We have also found, in an orthotopic transplantation model of diffuse-type gastric carcinoma OCUM-2MLN, that treatment with low-dose TβR-I inhibitor did not affect the extent of lymph node metastasis 16 days later.[8,43] Moreover, Ge et al reported that metastasis of certain breast tumors was prevented by TβR-I inhibitor through activation of immune function.[44]

Dendritic cells, cytotoxic T cells, and natural killer cells, which could be involved in antitumor immune responses, are known to be functionally inhibited by TGF-β signaling.[45] Dendritic cells are reported to migrate from sites of inflammation to regional lymph nodes through lymphatic vessels for presenting antigens to initiate further immune responses.[46,47] Therefore, it is possible that the use of TβR-I inhibitor may enhance antitumor immune responses via providing more routes for dendritic cells to migrate from tumors to regional lymph nodes and recovering functions of various immune cells, including dendritic cells inhibited by TGF-β ligands. These issues, however, remain for further investigation.

In conclusion, we have shown that inhibition of endogenous TGF-β signaling results in induction of lymphangiogenesis. Although TβR-I inhibitor induces lymphangiogenesis in the presence of VEGF-C and possibly via other lymphangiogenic cytokines, it remains to be determined whether it can induce the spread of tumors through lymphatic vessels or suppress it through activation of immune function.

Acknowledgments

The authors thank members of the Department of Molecular Pathology of the University of Tokyo for discussion.

This work was supported by KAKENHI (Grant-in-Aid for Scientific Research) from the Ministry of Education, Culture, Sports, Science and Technology of Japan.

Authorship

Contribution: M.O. performed the research and wrote the manuscript; C.I. collected data, contributed vital new reagents or analytical tools, and analyzed and interpreted the data; H.I.S. performed the research and collected the data; K.K. collected the data and contributed vital new reagents or analytical tools; Y.M. collected the data; T.W. contributed vital new reagents or analytical tools; A.K. collected the data; M.R.K. designed and performed the research, analyzed and interpreted the data, performed statistical analysis, and wrote the manuscript; K.M. designed the research, analyzed and interpreted the data, and wrote the manuscript.

Conflict-of-interest disclosure: The authors declare no competing financial interests.

Correspondence: Kohei Miyazono, Department of Molecular Pathology, Graduate School of Medicine, University of Tokyo, 7-3-1 Hongo, Bunkyo-ku, Tokyo 113-0033, Japan; e-mail: miyazono-ind@umin.ac.jp.

References

1. Heldin CH, Miyazono K, ten Dijke P. TGF-β signalling from cell membrane to nucleus through SMAD proteins. Nature. 1997;390:465-471.
2. Shi Y, Massague J. Mechanisms of TGF-β signaling from cell membrane to the nucleus. Cell. 2003;113:685-700.
3. Feng XH, Derynck R. Specificity and versatility in TGF-β signaling through Smads. Annu Rev Cell Dev Biol. 2005;21:659-693.
4. Bertolino P, Deckers M, Lebrin F, ten Dijke P. Transforming growth factor-β signal transduction in angiogenesis and vascular disorders. Chest. 2005;128:585S-590S.
5. Dickson K, Philip A, Warshawsky H, O'Connor-McCourt M, Bergeron JJ. Specific binding of endocrine transforming growth factor-β 1 to vascular endothelium. J Clin Invest. 1995;95:2539-2554.
6. Oshima M, Oshima H, Taketo MM. TGF-β receptor type II deficiency results in defects of yolk sac hematopoiesis and vasculogenesis. Dev Biol. 1996;179:297-302.
7. Larsson J, Goumans MJ, Sjostrand LJ, et al. Abnormal angiogenesis but intact hematopoietic potential in TGF-β type I receptor-deficient mice. EMBO J. 2001;20:1663-1673.
8. Kano MR, Bae Y, Iwata C, et al. Improvement of cancer-targeting therapy, using nanocarriers for intractable solid tumors by inhibition of TGF-β signaling. Proc Natl Acad Sci U S A. 2007;104:3460-3465.
9. Bierie B, Moses HL. Tumour microenvironment. TGF-β: the molecular Jekyll and Hyde of cancer. Nat Rev Cancer. 2006;6:506-520.
10. Mandriota SJ, Jussila L, Jeltsch M, et al. Vascular endothelial growth factor-C-mediated lymphangiogenesis promotes tumour metastasis. EMBO J. 2001;20:672-682.
11. Stacker SA, Caesar C, Baldwin ME, et al. VEGF-D promotes the metastatic spread of tumor cells via the lymphatics. Nat Med. 2001;7:186-191.
12. Kajiya K, Hirakawa S, Ma B, Drinnenberg I, Detmar M. Hepatocyte growth factor promotes lymphatic vessel formation and function. EMBO J. 2005;24:2885-2895.
13. Cao R, Bjorndahl MA, Religa P, et al. PDGF-BB induces intratumoral lymphangiogenesis and promotes lymphatic metastasis. Cancer Cell. 2004;6:333-345.
14. Tammela T, Saaristo A, Lohela M, et al. Angiopoietin-1 promotes lymphatic sprouting and hyperplasia. Blood. 2005;105:4642-4648.
15. Veikkola T, Alitalo K. Dual role of Ang2 in postnatal angiogenesis and lymphangiogenesis. Dev Cell. 2002;3:302-304.
16. Shin JW, Min M, Larrieu-Lahargue F, et al. Prox1 promotes lineage-specific expression of fibroblast growth factor (FGF) receptor-3 in lymphatic endothelium: a role for FGF signaling in lymphangiogenesis. Mol Biol Cell. 2006;17:576-584.
17. Shibuya M. Vascular endothelial growth factor receptor-2: its unique signaling and specific ligand, VEGF-E. Cancer Sci. 2003;94:751-756.
18. Cursiefen C, Chen L, Borges LP, et al. VEGF-A stimulates lymphangiogenesis and hemangiogenesis in inflammatory neovascularization via macrophage recruitment. J Clin Invest. 2004;113:1040-1050.
19. Veikkola T, Jussila L, Makinen T, et al. Signalling via vascular endothelial growth factor receptor-3 is sufficient for lymphangiogenesis in transgenic mice. EMBO J. 2001;20:1223-1231.
20. Karkkainen MJ, Haiko P, Sainio K, et al. Vascular endothelial growth factor C is required for sprouting of the first lymphatic vessels from embryonic veins. Nat Immunol. 2004;5:74-80.
21. Laakkonen P, Waltari M, Holopainen T, et al. Vascular endothelial growth factor receptor 3 is involved in tumor angiogenesis and growth. Cancer Res. 2007;67:593-599.
22. Hirakawa S, Brown LF, Kodama S, Paavonen K, Alitalo K, Detmar M. VEGF-C-induced lymphangiogenesis in sentinel lymph nodes promotes tumor metastasis to distant sites. Blood. 2007;109:1010-1017.
23. Oliver G. Lymphatic vasculature development. Nat Rev Immunol. 2004;4:35-45.
24. Wigle JT, Oliver G. Prox1 function is required for the development of the murine lymphatic system. Cell. 1999;98:769-778.
25. Wigle JT, Harvey N, Detmar M, et al. An essential role for Prox1 in the induction of the lymphatic endothelial cell phenotype. EMBO J. 2002;21:1505-1513.
26. Petrova TV, Makinen T, Makela TP, et al. Lymphatic endothelial reprogramming of vascular endothelial cells by the Prox-1 homeobox transcription factor. EMBO J. 2002;21:4593-4599.
27. Hong YK, Harvey N, Noh YH, et al. Prox1 is a master control gene in the program specifying lymphatic endothelial cell fate. Dev Dyn. 2002;225:351-357.
28. Mishima K, Watabe T, Saito A, et al. Prox1 Induces lymphatic endothelial differentiation via integrin α9 and other signaling cascades. Mol Biol Cell. 2007;18:1421-1429.
29. Nagy A, Rossant J, Nagy R, Abramow-Newerly W, Roder JC. Derivation of completely cell culture-derived mice from early-passage embryonic stem cells. Proc Natl Acad Sci U S A. 1993;90:8424-8428.
30. Suzuki H, Watabe T, Kato M, Miyazawa K, Miyazono K. Roles of vascular endothelial growth factor receptor 3 signaling in differentiation of mouse embryonic stem cell-derived vascular progenitor cells into endothelial cells. Blood. 2005;105:2372-2379.
31. Brunner AM, Marquardt H, Malacko AR, Lioubin MN, Purchio AF. Site-directed mutagenesis of cysteine residues in the pro region of the transforming growth factor β1 precursor. J Biol Chem. 1989;264:13660-13664.
32. Kreuger J, Nilsson I, Kerjaschki D, Petrova T, Alitalo K, Claesson-Welsh L. Early lymph vessel development from embryonic stem cells. Arterioscler Thromb Vasc Biol. 2006;26:1073-1078.
33. Liersch R, Nay F, Lu L, Detmar M. Induction of lymphatic endothelial cell differentiation in embryoid bodies. Blood. 2006;107:1214-1216.
34. Vlahakis NE, Young BA, Atakilit A, Sheppard D. The lymphangiogenic vascular endothelial growth factors VEGF-C and -D are ligands for the integrin α9β1. J Biol Chem. 2005;280:4544-4552.
35. Sawyer JS, Anderson BD, Beight DW, et al. Synthesis and activity of new aryl- and heteroaryl-substituted pyrazole inhibitors of the transforming growth factor-β type I receptor kinase domain. J Med Chem. 2003;46:3953-3956.
36. Laping NJ, Grygielko E, Mathur A, et al. Inhibition of transforming growth factor (TGF)-β 1-induced extracellular matrix with a novel inhibitor of the TGF-β type I receptor kinase activity: SB-431542. Mol Pharmacol. 2002;62:58-64.
37. Baluk P, Tammela T, Ator E, et al. Pathogenesis of persistent lymphatic vessel hyperplasia in chronic airway inflammation. J Clin Invest. 2005;115:247-257.
38. Goumans MJ, Valdimarsdottir G, Itoh S, et al. Activin receptor-like kinase (ALK)1 is an antagonistic mediator of lateral TGF-β/ALK5 signaling. Mol Cell. 2003;12:817-828.
39. Watabe T, Nishihara A, Mishima K, et al. TGF-β receptor kinase inhibitor enhances growth and integrity of embryonic stem cell-derived endothelial cells. J Cell Biol. 2003;163:1303-1311.
40. Gale NW, Prevo R, Espinosa J, et al. Normal lymphatic development and function in mice deficient for the lymphatic hyaluronan receptor LYVE-1. Mol Cell Biol. 2007;27:595-604.
41. Groger M, Loewe R, Holnthoner W, et al. IL-3 induces expression of lymphatic markers Prox-1 and podoplanin in human endothelial cells. J Immunol. 2004;173:7161-7169.
42. Carroll PA, Brazeau E, Lagunoff M. Kaposi's sarcoma-associated herpesvirus infection of blood endothelial cells induces lymphatic differentiation. Virology. 2004;328:7-18.
43. Iwata C, Kano MR, Komuro A, et al. Inhibition of cyclooxygenase-2 suppresses lymph node metastasis via reduction of lymphangiogenesis. Cancer Res. 2007;67:10181-10189.
44. Ge R, Rajeev V, Ray P, et al. Inhibition of growth and metastasis of mouse mammary carcinoma by selective inhibitor of transforming growth factor-β type I receptor kinase in vivo. Clin Cancer Res. 2006;12:4315-4330.
45. Wrzensinski SH, Wan YY, Flavell RA. Transforming growth factor-β and the immune response: implications for anticancer therapy. Clin Cancer Res. 2007;13:5262-5270.
46. Halin C, Tobler NE, Vigl B, Brown LF, Detmar M. VEGF-A produced by chronically inflamed tissue induces lymphangiogenesis in draining lymph nodes. Blood. 2007;110:3158-3167.
47. Angeli V, Ginhoux F, Llodra J, et al. B cell-driven lymphangiogenesis in inflamed lymph nodes enhances dendritic cell mobilization. Immunity. 2006;24:203-215.

Improvement of cancer-targeting therapy, using nanocarriers for intractable solid tumors by inhibition of TGF-β signaling

Mitsunobu R. Kano*†‡, Younsoo Bae‡§, Caname Iwata*¶, Yasuyuki Morishita*, Masakazu Yashiro‖, Masako Oka*, Tomoko Fujii*, Akiyoshi Komuro*, Kunihiko Kiyono*, Michio Kaminishi¶, Kosei Hirakawa‖, Yasuyoshi Ouchi†, Nobuhiro Nishiyama§**, Kazunori Kataoka‡§**††, and Kohei Miyazono*‡‡

Departments of *Molecular Pathology, †Geriatrics, ¶Gastrointestinal Surgery, and §Center for Disease Biology and Integrative Medicine, Graduate School of Medicine; **Department of Materials Engineering, Graduate School of Engineering; and ‡Center for Nano-Bio Integration, University of Tokyo, Tokyo 113-0033 Japan; and ‖Department of Surgical Oncology, Osaka City University Graduate School of Medicine, Osaka 545-8585, Japan

Communicated by Tadatsugu Taniguchi, University of Tokyo, Tokyo, Japan, December 28, 2006 (received for review December 25, 2006)

Transforming growth factor (TGF)-β plays a pivotal role in regulation of progression of cancer through effects on tumor microenvironment as well as on cancer cells. TGF-β inhibitors have recently been shown to prevent the growth and metastasis of certain cancers. However, there may be adverse effects caused by TGF-β signaling inhibition, including the induction of cancers by the repression of TGF-β-mediated growth inhibition. Here, we present an application of a short-acting, small-molecule TGF-β type I receptor (TβR-I) inhibitor at a low dose in treating several experimental intractable solid tumors, including pancreatic adenocarcinoma and diffuse-type gastric cancer, characterized by hypovascularity and thick fibrosis in tumor microenvironments. Low-dose TβR-I inhibitor altered neither TGF-β signaling in cancer cells nor the amount of fibrotic components. However, it decreased pericyte coverage of the endothelium without reducing endothelial area specifically in tumor neovasculature and promoted accumulation of macromolecules, including anticancer nanocarriers, in the tumors. Compared with the absence of TβR-I inhibitor, anticancer nanocarriers exhibited potent growth-inhibitory effects on these cancers in the presence of TβR-I inhibitor. The use of TβR-I inhibitor combined with nanocarriers may thus be of significant clinical and practical importance in treating intractable solid cancers.

angiogenesis | gastric cancer | molecular targeting therapy | pancreatic cancer

Chemotherapy that uses nanocarriers has been developed to improve the clinical treatment of solid tumors by obtaining high accumulation of drugs in tumor tissues but limited accumulation in normal organs. Doxil (1), a liposomal adriamycin (ADR), is one such drug that has already been used clinically (2). Doxil has exhibited therapeutic effects on some cancers with hypervascular characteristics (3, 4), including Kaposi sarcoma and ovarian cancers. Another promising formulation of nanocarriers is polymeric micelles (5, 6), which are already being used in clinical trials (7, 8).

However, despite the urgent need for effective chemotherapy for intractable solid tumors, including pancreatic adenocarcinoma (9) and diffuse-type gastric carcinoma (10), nanocarriers of any design have not been successful yet in exhibiting significant therapeutic effects on these cancers. Pancreatic cancer is the fourth leading cause of cancer-related death in the United States and the fifth in Japan (9), and the median survival period of patients who suffer from advanced pancreatic adenocarcinoma is still extremely short ($\approx$6 months), despite recent progress in development of conventional chemotherapies (11). Although cancer cells derived from these tumors are sufficiently sensitive *in vitro* to conventional anticancer agents such as ADR (12), most of these agents have failed to exhibit sufficient therapeutic effects *in vivo*, regardless of formulation, whether encapsulated in nanocarriers or not. The theoretical basis of the specific accumulation of nanocarriers in tumor tissues is leakiness of tumor vessels to the macromolecular agents, termed the "enhanced permeability and retention (EPR) effect," which was demonstrated and named by Maeda *et al.* (13, 14). The major obstacles to treatment of these cancer cells could thus be insufficient EPR effect because of certain characteristics of their cancer microenvironment, including hypovascularity and thick fibrosis (15, 16). However, methods of regulating this effect have not been well investigated.

Transforming growth factor (TGF)-β signaling plays a pivotal role in both the regulation of the growth and differentiation of tumor cells and the functional regulation of tumor interstitium (17). Because TGF-β is a multifunctional cytokine that inhibits the growth of epithelial cells and endothelial cells and induces deposition of extracellular matrix, inhibition of TGF-β signaling in cancer cells and fibrotic components has been expected to facilitate the effects of anticancer therapy. TGF-β binds to type II (TβR-II) and type I receptors (TβR-I), the latter phosphorylates Smad2 and −3. Smad2 and −3 then form complexes with Smad4, translocate into the nucleus, and regulate the transcription of target genes (18). Several small-molecule TβR-I inhibitors have been reported to prevent metastasis of some cancers (19). However, there may be adverse effects of TGF-β inhibition, including potential progression of some cancers because of the repression of TGF-β-mediated growth inhibition of epithelial cells (20).

In this study, we show that administration of the small-molecule TβR-I inhibitor (LY364947) (21) at a low dose, which could minimize the potential side effects of TβR-I inhibitor, can alter the tumor microenvironment and enhance the EPR effect. This effect of low-dose TβR-I inhibitor was demonstrated with two of nanocarriers, i.e., Doxil and a polymeric micelle incorporating ADR (micelle ADR) that we have recently developed (22) [supporting information (SI) Fig. 7]. The present findings strongly suggest that our method, which uses a combination of

Author contributions: M.R.K., K. Kataoka, and K.M. designed research; M.R.K., Y.B., C.I., Y.M., M.O., T.F., A.K., and K. Kiyono performed research; M.Y. and K.H. contributed new reagents/analytic tools; M.R.K., Y.B., C.I., M.K., Y.O., N.N., K. Kataoka, and K.M. analyzed data; and M.R.K., N.N, K. Kataoka, and K.M. wrote the paper.

The authors declare no conflict of interest.

Freely available online through the PNAS open access option.

Abbreviations: ADR, adriamycin; EPR, enhanced permeability and retention; PECAM, platelet/endothelial cell adhesion molecule; TβR-I, type I transforming growth factor β receptor.

††To whom correspondence may be addressed at: Department of Material Engineering, Graduate School of Engineering, University of Tokyo, Tokyo 113-8656, Japan. E-mail: kataoka@bmw.t.u-tokyo.ac.jp.

‡‡To whom correspondence may be addressed. E-mail: miyazono-ind@umin.ac.jp.

This article contains supporting information online at www.pnas.org/cgi/content/full/0611660104/DC1.

www.pnas.org/cgi/doi/10.1073/pnas.0611660104

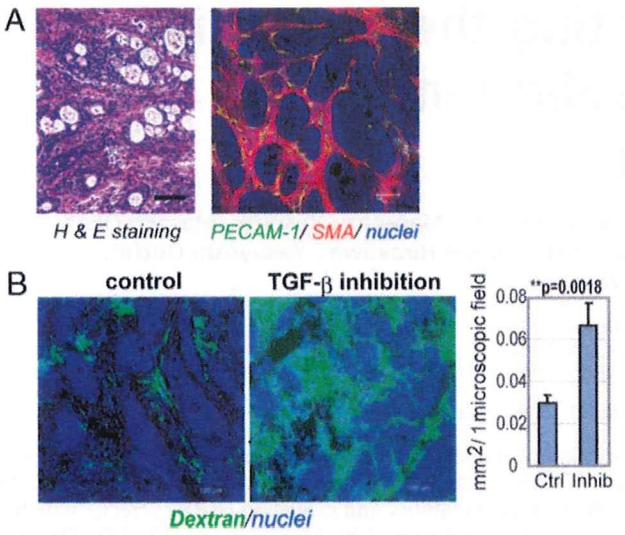

Fig. 1. Histology of BxPC3 xenograft and effects of low-dose TβR-I inhibitor. (*A*) The histology of the TGF-β-nonresponsive BxPC3 xenograft, used as a model of poorly differentiated pancreatic adenocarcinoma, shown in H&E staining and immunohistochemistry. Examination revealed nests of tumor cells in gland-like structures, with areas rich in fibrotic components (filled by α-smooth muscle actin (SMA)-positive myofibroblasts, shown in red) between them. The tumor tissue also includes some PECAM-1-positive vessels (shown in green) in the interstitium, although almost no vasculature was observed inside the nests of tumor cells. (*B*) Dextran leakage. At 24 h after administration of low-dose TβR-I inhibitor (1 mg/kg i.p.), i.v.-administered dextran of 2 MDa (50 nm in hydrodynamic diameter) exhibited broader distribution with 1 mg/kg TβR-I inhibitor (*Right*) than in the control (*Left*), which was quantified and shown in the graph ($n = 12$). Error bars in the graphs represent standard errors, and *P* values were calculated by Student's *t* test. Ctrl, control; Inhib, inhibitor. (Scale bars, 100 μm.)

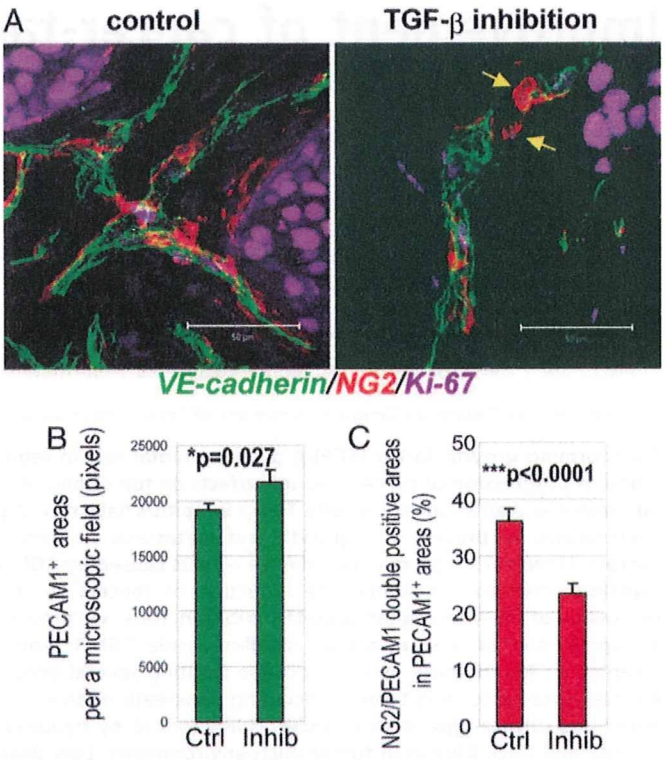

Fig. 2. Morphological changes in cancer neovasculature at 24 h after administration of low-dose TβR-I inhibitor. (*A*) Immunostaining of the tumor neovasculature. NG2-positive pericytes (shown in red) were dissociated (yellow arrows in *Right*) from VE-cadherin-positive endothelium (shown in green) after TβR-I inhibitor treatment for 24 h. (Scale bars, 50 μm.) (*B* and *C*) Areas of PECAM-1-positive endothelium (*B*) and pericyte-coverage (*C*) were quantified ($n = 40$) and are shown in the graphs. Error bars in the graphs represent standard errors, and *P* values were calculated by Student's *t* test. Ctrl, control; Inhib, inhibitor.

low-dose small molecule TβR-I inhibitor and long-circulating nanocarriers, is a promising way to treat intractable cancers.

Results

We used the xenografted BxPC3 human pancreatic adenocarcinoma cell line in nude mice as a disease model (Fig. 1). BxPC3 cells do not respond to TGF-β, because of lack of functional Smad4. Hematoxylin/eosin (H&E) staining of tumor tissue in this model (Fig. 1*A Left*) revealed poorly differentiated histology, with a certain number of blood vessels and thick fibrotic tissue in the interstitium. There was, however, almost no vasculature inside of tumor cell nests (Fig. 1*A Right*). This model thus represents the histological characteristics of some intractable solid tumors.

Systemic administration of low-dose TβR-I inhibitor in this model significantly altered the characteristic of tumor vasculature at 24 h after administration. We investigated the functional aspects of the effects of low-dose TβR-I inhibitor, using i.v.-administered large-molecule dextran of 2 MDa with a hydrodynamic diameter of 50 nm (23, 24), which is equivalent to the common sizes of nanocarriers (Fig. 1*B*). Although dextran of this molecular size for the most part remained in the intravascular space in the control condition, as reported in ref. 24, the use of TβR-I inhibitor resulted in a far broader distribution of this macromolecule around the tumor neovasculature. These findings suggest that low-dose TβR-I inhibitor can maintain blood flow in the tumor vasculature and simultaneously induce extravasation of macromolecules.

To investigate the mechanisms of effect of TβR-I inhibitor on the neovasculature, we analyzed the changes in three major components of tumor vasculature, i.e., endothelium, pericytes (Fig. 2), and basement membrane (SI Fig. 8), at 24 h after administration of TβR-I inhibitor. The areas of vascular endothelial cells stained by platelet/endothelial cell adhesion molecule (PECAM)-1 increased slightly with TβR-I inhibitor treatment (Fig. 2*B*). Although pericyte-coverage of endothelium has been reported to be incomplete in tumors (25), coverage of the endothelium by pericytes, which were determined as NG2-positive perivascular cells, was further decreased by the TβR-I inhibitor treatment. This finding was confirmed by comparing the ratios of PECAM-1/NG2-double-positive areas to PECAM-1-positive areas (Fig. 2*C*). On the other hand, vascular basement membrane, which was determined by staining with collagen IV, did not differ significantly in the presence or absence of TβR-I inhibitor (SI Fig. 8). We also examined the vasculature in normal organs and found that it was not affected by TβR-I inhibitor in terms of permeability of 2-MDa dextran and morphology on immunostaining (SI Fig. 9).

We next examined the effects of i.p. administration of small-molecule TβR-I inhibitor at a low dose (1 mg/kg) on TGF-β signaling, by determining phosphorylation of Smad2 (SI Figs. 10 and 11). Because it is a small-molecule agent, TβR-I inhibitor transiently suppressed phosphorylation of Smad2. In nucleated blood cells, phosphorylation of Smad2 was significantly suppressed at 1 h after administration of TβR-I inhibitor, but it gradually recovered toward 24 h. In contrast, phosphorylation of Smad2 in tumor cells and most interstitial cells was not suppressed even 1 h after administration, whereas a higher dose (25 mg/kg) of TβR-I inhibitor inhibited Smad2 phosphorylation in most tumor cells. Accordingly, the extent of fibrosis in cancer xenografts treated with low-dose TβR-I inhibitor did not differ

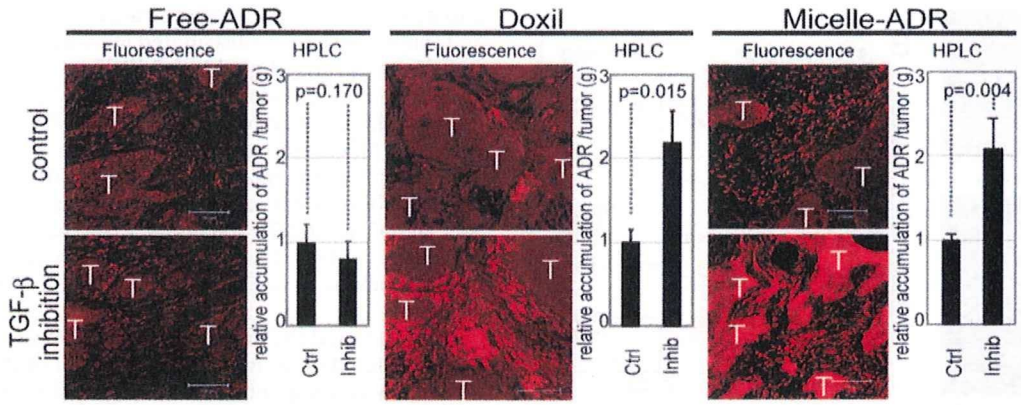

Fig. 3. Biodistribution of ADR in the BxPC3 model. The biodistribution of ADR was investigated in the BxPC3 model by fluorescence examination (T indicates nests of tumor cells in tumor tissues) and by HPLC. The distributions of Doxil, micelle ADR, and free ADR at 8 mg/kg with and without TβR-I inhibitor at 1 mg/kg were examined 24 h after administration. Enhancement of drug accumulation in tumor was specifically observed with TβR-I inhibitor with Doxil and micelle ADR. Error bars in the graphs represent standard errors, and *P* values were calculated by Student's *t* test. Ctrl, control; Inhib, inhibitor.

from that in the control (SI Fig. 12). On the other hand, low-dose TβR-I inhibitor specifically suppressed the phosphorylation of Smad2 in vascular endothelium (SI Fig. 11*B*). These findings suggest that the use of small-molecule TβR-I inhibitor at low doses is advantageous for limiting adverse effects.

We thus hypothesized that low-dose TβR-I inhibitor may enhance the accumulation of nanocarriers, the molecular sizes of which are similar to 2-MDa dextran, in hypovascular solid tumors. We used two nanocarriers to test this hypothesis: Doxil (26), a liposomal ADR, and a core–shell type polymeric micelle-encapsulating ADR (micelle ADR) that we developed (22). The latter is a micellar nanocarrier consisted of block copolymers in which ADR is conjugated to the PEG chain through an acid–labile linkage. This drug carrier releases free ADR molecules selectively in acidic conditions, e.g., in intracellular endosomes and lysosomes (SI Fig. 7). We tested the effects of i.p. administration of TβR-I inhibitor with i.v. administration of Doxil or micelle ADR at 8 mg/kg on size-matched xenografts of BxPC3 cells, which are ADR-sensitive *in vitro* (12). Conventional ADR without drug carriers (free ADR), a small-molecule compound of MW 543.52, was also used for comparison. We first examined the distribution of ADR molecules in tumor tissues by using confocal imaging of fluorescence of ADR and HPLC (Fig. 3). The fluorescence of ADR molecules in micelle ADR is detectable only when ADR molecules are released from the micelle, whereas that in Doxil is detectable even when it is encapsulated in the liposome. The total amount of accumulated ADR, the sum of that in cancer cells and the cancer microenvironment, is measured by HPLC, which detects ADR molecules with and without drug carriers. Administration of TβR-I inhibitor with the nanocarriers yielded significant enhancement of intratumoral accumulation of ADR molecules. Because TβR-I inhibitor did not increase the accumulation of free ADR, we suspected that only macromolecules would be benefited by the use of TβR-I inhibitor through enhancement of EPR effect.

We then examined the growth-inhibitory effects of these anticancer drugs with and without TβR-I inhibitor on size-matched BxPC3 xenografts. As shown in Fig. 4*A*, the growth curves of the BxPC3 xenografts confirmed the findings for the distribution of ADR molecules. None of free ADR, Doxil, micelle ADR as monotherapy, or free ADR with TβR-I inhibitor significantly reduced tumor growth. In contrast, ADR encapsulated in nanocarriers exhibited significant effects on the growth of tumor when combined with TβR-I inhibitor (see *SI List* for statistical study).

Because micelle ADR was more effective than Doxil (as shown in Figs. 3 and 4*A*), and the maximum tolerated dose of micelle ADR is far higher than one shot of 8 mg/kg (22, 26) (the dose in Fig. 4*A*), we further tested the growth-inhibitory effects of an increased dose of micelle ADR combined with TβR-I inhibitor (Fig. 4*B*). When micelle ADR or free ADR was

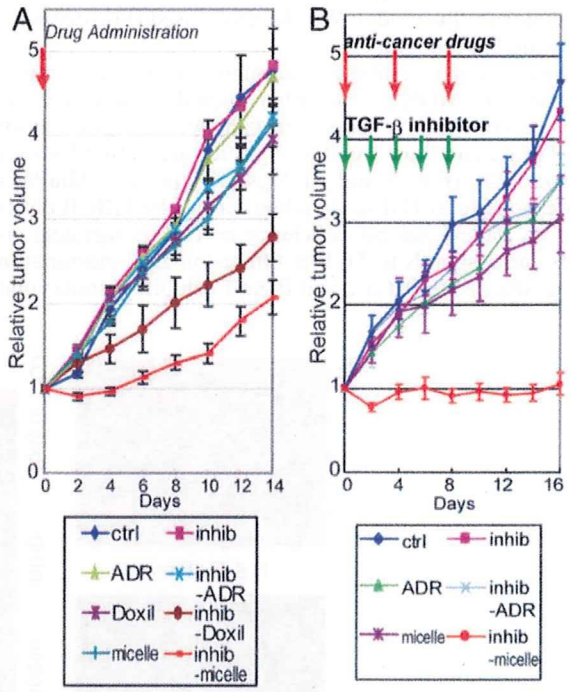

Fig. 4. Effects of TβR-I inhibitor on anti-tumor activity of nanocarriers, incorporating ADR in the BxPC3 model. (*A*) Free ADR, liposomal ADR (Doxil), micelle ADR (micelle) or vehicle control (ctrl) was administered i.v. in a single bolus with and without TβR-I inhibitor (inhib) i.p. to xenografted mice in which tumors had been allowed to grow for a few weeks before treatment ($n = 5$). Relative tumor sizes were measured every second day and are shown as a growth curve with bars showing standard errors. Only nanocarriers administered together with TβR-I inhibitor exhibited significant reduction of growth compared with the control. (*B*) Growth curve study with an increased dose of micelle ADR. With the day of initiation of drug administration designated day 0, anticancer drugs were administered i.v. on days 0, 4, and 8 with and without i.p. TβR-I inhibitor on days 0, 2, 4, 6, and 8. Further growth-inhibitory effect was observed with an increase in dose of micelle ADR. (Results of multivariate ANOVA study are shown in *SI List*.)

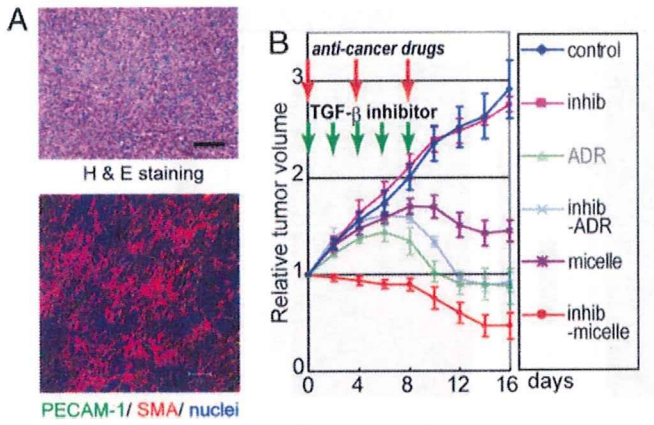

Fig. 5. Growth-curve study in the MiaPaCa-2 pancreatic cancer xenograft model. (*A*) TGF-β-nonresponsive MiaPaCa-2 cell xenografts exhibited an undifferentiated pattern of histology on H&E staining (*Upper*), with rich SMA-positive fibrotic tissue (show in red in *Lower*) and much less PECAM-1-positive vasculature (shown in green) compared with the BxPC3 model. (*B*) The same experimental protocol as in Fig. 4*B* was used in the model, and the effectiveness of the use of TβR-I inhibitor was confirmed. Inhib, inhibitor; micelle, micelle-ADR. (Results of multivariate ANOVA for the growth-curve studies are shown in *SI List*.)

administered on days 0, 4, and 8, with and without TβR-I inhibitor, only micelle ADR administered together with TβR-I inhibitor exhibited nearly complete growth-inhibitory effect on the tumor in this model. We therefore used this regimen in the following experiments.

The efficacy of combined treatment was further confirmed by using micelle ADR in two other animal models of pancreatic adenocarcinoma. We used size-matched xenograft models of MiaPaCa-2 and Panc-1 cell lines, which are both ADR-sensitive *in vitro* (12) (Fig. 5 and SI Figs. 13 and 14). MiaPaCa-2 is nonresponsive to TGF-β signaling because of TβR-II deficiency, whereas Panc-1 has no deficiency in TGF-β signaling components and responds to TGF-β. On histological examination, the xenografts of MiaPaCa-2 and Panc-1 exhibited similar undifferentiated pattern with scattered cancer cells, rich fibrous tissue, and sparse vasculature distributed homogeneously, unlike that of BxPC3 xenografts (Fig. 5*A* and SI Fig. 14*A*). Use of low-dose TβR-I inhibitor in these models again significantly enhanced the growth-inhibitory effects of micelle ADR (see Fig. 5*B*, SI Fig. 14*B*, and *SI List* for statistical analyses). Effects of free ADR were again not enhanced by TβR-I inhibitor, although the drug itself exhibited some degree of growth-inhibitory effect on the MiaPaCa-2 xenografts. Analysis of the biodistribution of ADR molecules (SI Figs. 13 and 14 *C* and *D*) confirmed the effects of TβR-I inhibitor on accumulation of micelle ADR in these cancer models.

We also tested the growth-inhibitory effect of TβR-I inhibitor and micelle ADR in an orthotopic model of the OCUM-2MLN cell line, which responds to TGF-β (27) (Fig. 6). OCUM-2MLN was derived from a patient with another intractable solid tumor, diffuse-type gastric cancer. The cancer cells were implanted in the gastric wall of nude mice and allowed to grow *in situ* for 2 weeks, leading to formation of hypovascular and fibrotic tumors in the gastric wall (Fig. 6*A*). Tumor area (framed by arrowheads in Fig. 6*B*, *Left*) was measured before the initiation of drug administration, and tumor growth was evaluated by calculating the relative tumor area at day 16 by measuring tumor area again (Fig. 6*B*, *Right*). Significant reduction of tumor growth was again observed only in the mice treated with TβR-I inhibitor and micelle ADR. The distribution of ADR, as detected by fluorescence, confirmed this growth-inhibitory effect (data not shown). These findings suggest that the use of TβR-I inhibitor may enhance the accumulation of nanocarriers in hypovascular solid tumors.

Finally, we examined whether low-dose TβR-I inhibitor increases EPR effect specifically in tumor tissues and not in normal organs. Although nanocarriers were originally designed to decrease the drug accumulation in normal organs, it is important to determine whether use of TβR-I inhibitor exacerbates their side effects (SI Fig. 15). In liver, spleen, kidney, blood, and heart, accumulation of ADR as determined by HPLC was not significantly increased by TβR-I inhibitor (SI Fig. 15 *A* and *B*). Neither dermatitis nor phlebitis around the tail veins was exacerbated by addition of TβR-I inhibitor (SI Fig. 15*C*). In addition, the weight

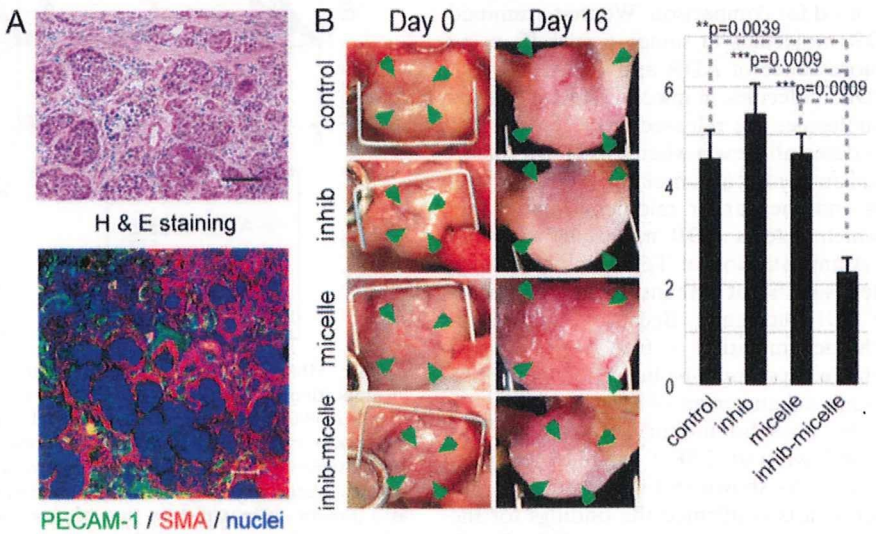

Fig. 6. Effects of TβR-I inhibitor administered together with micelle ADR in an orthotopic diffuse-type gastric cancer model. OCUM-2MLN, a human diffuse-type gastric cancer cell line, was inoculated into the gastric wall of nude mice ($n = 5$). Two weeks after inoculation, the cancer tissues exhibited diffuse-type histology on H&E staining (*A Upper*) with sparse formation of blood vessels (PECAM-1 staining, shown in green) (*A Lower*). The sizes of tumors on the gastric wall were measured based on tumor areas (*B Left*), and the values on day 16 were divided by those on day 0, the day of initiation of drug administration, to obtain relative tumor areas. Relative tumor areas are shown with bars for standard errors (*B Right*). TβR-I inhibitor significantly reduced tumor growth in this model, as well. *P* values were calculated by Student's *t* test. Inhib, inhibitor; micelle, micelle-ADR.